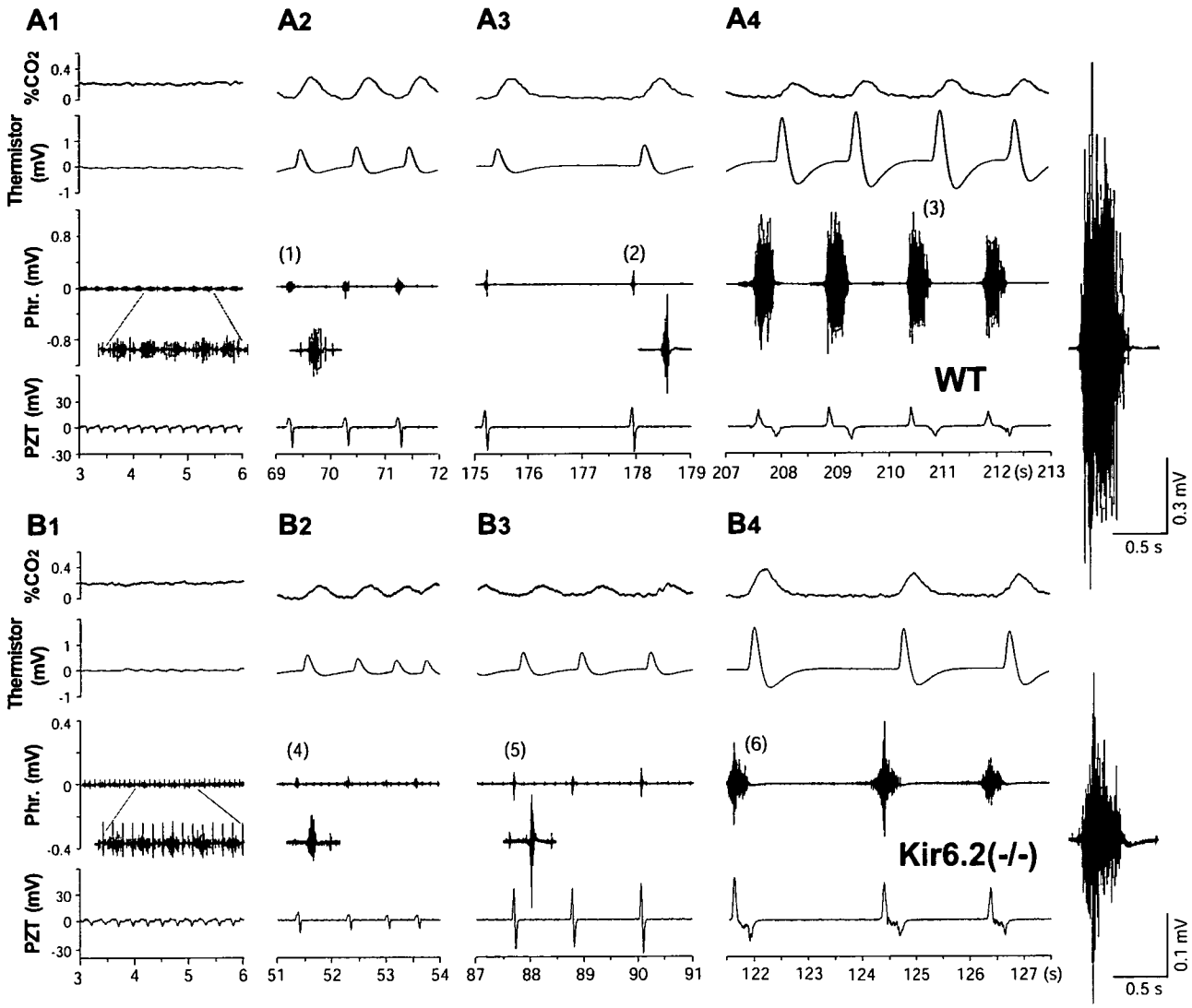

FIG. 8. Details of respiratory responses of wild-type (WT) (A) and knockout (KO) (B) mice during prolonged hypoxia at time points marked in Fig. 7. (A1) Control breaths before hypoxic challenge. The third trace represents phrenic nerve discharges. Note that the piezoelectric transducer (PZT) responses show asymmetrical shape. (A2) Typical traces during depression. The amplitude of percentage CO_2 and thermistor response was greatly increased. Responses numbered above are enlarged in insets. Note that PZT responses show asymmetrical shape during depression. The upward PZT deflection of wide duration and intermediate amplitude correlates well with the phrenic discharge above. (A3) A typical example of breaths during the stable, slow respiration, characterized by short width, relatively large amplitude phrenic discharge and PZT response of biphasic symmetrical shape. (A4) Terminal breaths characterized by phrenic discharge are much wider than other breaths and have extremely large amplitude. The shape of PZT response of terminal breaths is distinct from others during the preceding hypoxic period. Ordinates shown in A1 are common to A2–4. Scales for the phrenic discharge in the rightmost inset are common to other insets in A. (B1–4) Similar to A1–4 but of a KO mouse. Phr., phrenic nerve recording; PZT, piezoelectric transducer.

In KO mice, both the duration of depression and persistent gasping were much shorter than in wild-type mice (Figs 9, B2 and C2, and 10, A2 and B2), and the onset of terminal gasping was significantly earlier than in wild-type mice (Figs 9, C2, and 10, C1). The duration of terminal gasping was also significantly shorter in KO than in wild-type mice (Fig. 10, C2), indicating a crucial role of the K_{ATP} channels in the maintenance of depression and persistent and terminal gasping in the anesthetized condition.

Hypoxia-induced respiratory changes in unanesthetized condition

Hypoxic responses were also analysed under unanesthetized condition to exclude the influence of anesthesia. In preliminary tests, all wild-type and half of the KO mice exhibited no gasps at 8–9% O_2 within the recording period (1500 s). Below 4% O_2, or if the hypoxia was introduced as rapidly as in the anesthetized experiments, generalized convulsive seizure interfered with the detection of gasping in KO mice (Yamada *et al.*, 2001). Thus, the experiments were performed at O_2 concentrations from 4.5 to 7.0% at a very slowly declining rate of O_2 while CO_2 changes and body movement were monitored (see Materials and methods).

In these conditions, changes in the respiratory frequency could readily be detected by the PZT responses (see Materials and methods), the shapes of which were essentially similar to those detected in anesthetized condition (Fig. 11, A1 and B1). Tachypnea (onset, open arrowhead in Fig. 11, A2 and B2) and subsequent depression (onset, filled arrow in Fig. 11, A2 and B2) were detected in both wild-type and KO mice. At 4.5–5.0% O_2, no significant difference in onset of tachypnea was detected between wild-type and KO mice, as in the

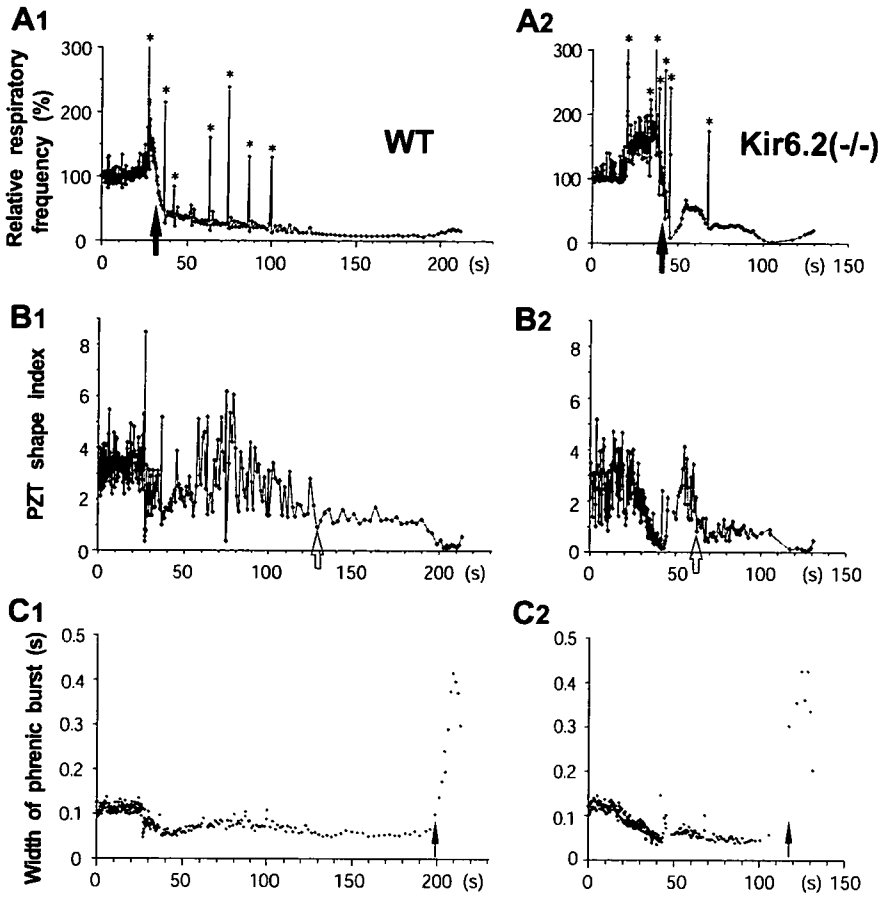

FIG. 9. Quantitative analyses of the respiratory responses of wild-type (WT) (A1, B1 and C1) and knockout (KO) (A2, B2 and C2) mice during prolonged hypoxia depicted in Fig. 7. Changes in the respiratory frequency relative to the mean frequency before hypoxic challenge (0–10 s) of WT (A1) and KO (A2) mice. The onset of depression in KO mice (filled arrow in A2) was delayed compared with WT (filled arrow in A1). In these plots, respiratory frequency was counted by piezoelectric transducer (PZT) deflections with reference to expiratory flow. Asterisks indicate transient tachypnea around extraordinarily large breaths (sighs). (B1 and B2) Similar to A but changes in the PZT index, reflecting symmetry of the upward (inspiration) and downward (expiration) deflections of the PZT response. Open arrows indicate the time point at which the shape index shows a relatively constant value close to 1, i.e. the beginning of persistent gasping. For convenience, values in A and B (but not C) are connected by lines. (C1 and C2) Similar to A but changes in width of phrenic burst. An abrupt increase in the width is clear (thin arrows), suggesting that gasping of a distinct type begins (terminal gasping). Note the blank in the trace in C2, which indicates the apneic period before terminal gasping in KO mice.

anesthetized experiments (Fig. 12A). A similar correspondence was also detected in other concentration ranges (data not shown). In addition, unlike the anesthetized condition, no difference in peak period or maximal respiratory frequency of tachypnea ($P = 0.91$ and 0.58, respectively) was detected between wild-type ($n = 6$) and KO ($n = 4$) mice at 4.5–5.0% O_2, at which no significant difference in respiratory frequency was detected before hypoxic challenge. Consistently, the onset of depression that emerged after the tachypnea was also similar in the two types of mice (Fig. 12B).

One of the most distinctive features of the respiratory responses of wild-type mice in the unanesthetized condition was that the first half of the hypoxic period comprised irregularly mixed depressions of variable frequency (filled arrowheads in Fig. 11, A2) and apnea-like periods (open squares in Fig. 11, A2; very low amplitude in percentage CO_2 and PZT traces in Fig. 11, A1), frequently accompanied by large body movements (Fig. 11, A1, large deflections in PZT trace). Imprecise discrimination of depressions and apnea-like periods made evaluation of the total period of depression difficult; nevertheless, the responses could be discerned by changes in the respiratory frequency (Fig. 11, A2) and differences in the height of the percentage CO_2 trace in comparison with the PZT response (Fig. 11, A1). In fact, the duration of depression including the apnea-like period in wild-type mice (summation of the initial depression shown in Fig. 11, A2 with the periods indicated by filled arrowheads and open squares) was longer than in KO mice (estimated as in Fig. 11, B2).

Despite the irregularity in the hypoxic responses, a stable, slow respiration rhythm having a PZT shape distinct from that in the initial half of the hypoxic period eventually emerged in all wild-type mice tested [Fig. 11, A1, inset (1)]. This slow respiration exhibited a PZT response of either symmetrical biphasic [Fig. 11, A1, inset (1)] or triphasic [Fig. 11, A1, asterisk in inset (2)] shape and persisted until just before the terminal breaths [Fig. 11, A1, inset (3)]. The biphasic PZT shape was similar to that of the persistent gasping in anesthetized condition (Fig. 8, A3). However, the triphasic shape was produced by body movement possibly reflecting an expiration/inspiration/expiration sequence. As the biphasic and triphasic shapes emerged unpredictably during the hypoxic period, we included both types as persistent gasping in the present study.

The PZT shape of the terminal breaths in wild-type mice was similar to that in terminal gasping in anesthetized experiments, especially the long duration between positive and negative deflections [inset (3) in Fig. 11, A1; see also PZT trace in Fig. 8, A4], and in most cases a sharp deflection followed by a wide valley in the opposite direction. In addition, there was a clear tendency to a hypoxic response in accord

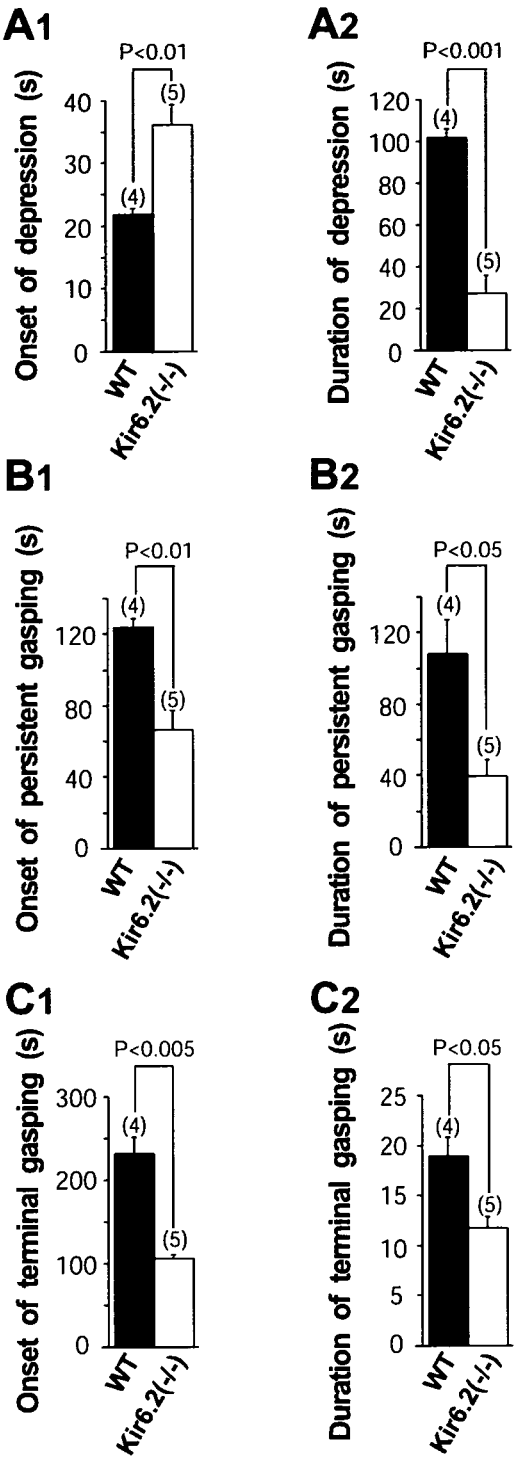

FIG. 10. Statistical comparison of depression (A), persistent gasping (B) and terminal gasping (C) under prolonged severe (5.0% O_2 at 60 s after valve opening) hypoxia between wild-type (WT) and knockout (KO) mice in anesthetized condition. (A1 and A2) Onset and duration of depression, respectively. (B1 and B2) Similar to A but of persistent gasping. Note that onset of depression in KO mice was significantly delayed by ~15 s from that in WT mice (A1) but the duration of depression in KO mice was shorter by ~80 s than in WT mice (A2), resulting in earlier onset of persistent gasping in KO than in WT mice (B1). (C1 and C2) Similar to A but of terminal gasping. As the duration of persistent gasping of KO mice was much shorter than in WT mice (B2), onset of terminal gasping of KO mice was significantly earlier than in WT mice (C1). Duration of terminal gasping of KO mice was slightly but significantly shorter than that of WT mice (C2). Onset was measured from the time that O_2 concentration actually began to decrease.

with the severity of the hypoxia in wild-type mice. The onset of the terminal gasping declined nearly linearly as the O_2 concentration was lowered within the range of testing (4.5–7.0% O_2) (Fig. 12D, correlation coefficient 0.87).

The KO mice also showed persistent and terminal gasping [insets (2) and (3), respectively, in Fig. 11, B1]. However, the period of stable gasping seldom persisted [compare inset (1) to (3) in Fig. 11, A1 and B1]. In addition, the onset of terminal gasping in KO mice was significantly earlier than in wild-type mice (Fig. 12C) and did not change regardless of the O_2 concentration (Fig. 12D, correlation coefficient 0.21), indicating an inability of the KO mice to regulate the hypoxic response according to the severity of the hypoxia in that range of O_2 concentration (see also Supplementary material, Fig. S1).

As mentioned, there was no difference in onset or duration (peak period) of tachypnea in wild-type and KO mice. In addition, the onset of initial depression was similar in both types of mice. Thus, the dependency of onset of terminal gasping on the severity of hypoxia (Fig. 12D) suggests that maintenance of hypoxic responses from onset of depression to the end of persistent gasping is regulated in an O_2-level-sensitive manner in wild-type but not KO mice. Thus, considering both the anesthetized and unanesthetized experiments, it is clear that Kir6.2-containing K_{ATP} channels are critically involved in the maintenance of depression and gasping during severe hypoxic conditions.

Discussion

Gasping appears clinically when the blood O_2 content is reduced to ~25% of the normal level, and is readily distinguished from eupnea by the large opening of the lower jaw and long interbreath interval. This distinct breathing pattern can persist for minutes or hours, assuring minimum ventilation until the blood oxygenation state is improved, but the molecular basis of the maintenance of gasping is poorly understood. In the present study, each of the hypoxic responses seen in wild-type mice could be generated in Kir6.2 KO mice but the duration of depression and gasping, and not of tachypnea and sigh was significantly shorter in KO than in wild-type mice in the anesthetized condition. In addition, the total duration from onset of depression to terminal gasping in KO mice was unaltered by the O_2 deprivation level within the range of testing (4.5–7.0% O_2) in unanesthetized condition, whereas total duration clearly depended upon the severity of the hypoxia in wild-type mice.

Contribution of central vs. peripheral ATP-sensitive potassium channels in hypoxia-induced respiratory responses

As KO mice lack K_{ATP} channels in the whole body, involvement of the peripheral K_{ATP} channels in the control of severe hypoxia-induced respiratory responses including gasping cannot be excluded. In particular, heart and skeletal muscle K_{ATP} channels, consisting of Kir6.2 and SUR2A subunits (Inagaki *et al.*, 1996), might contribute to the hypoxic responses. However, the difference in gasping between the wild-type and KO isolated head cannot be explained by the cardiac K_{ATP} channels. In addition, mice lacking vascular smooth muscle-type K_{ATP} channels containing Kir6.1 subunits exhibited gasping responses similar to those of wild-type mice when decapitated, suggesting that the Kir6.2-containing K_{ATP} channels in the central nervous system are crucial in the regulatory mechanism of gasping. Indeed, it has been reported that the time to last gasp following decapitation and that following exposure to systemic anoxia are similar in newborn rats when the body temperature is equalized (Fewell, 2005), indicating the

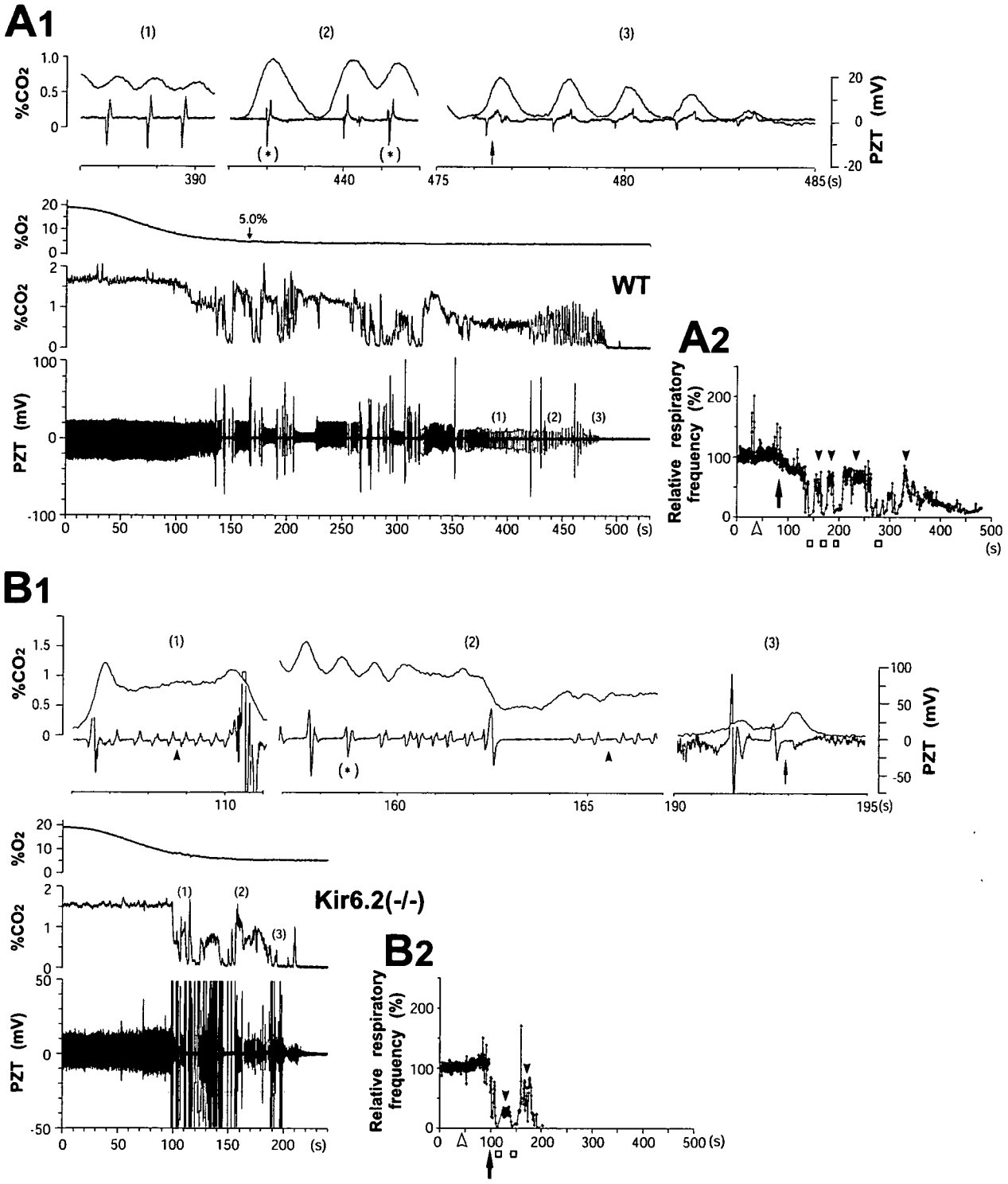

FIG. 11. Typical changes in respiration of mice subjected to severe hypoxia (4.5–5.0% O_2) in unanesthetized condition. Raw traces of respiratory responses (A1) and changes in the respiratory frequency relative to the mean frequency before hypoxic challenge (A2) of wild-type (WT) mouse subjected to 4.8% O_2. Hypoxia was imposed very slowly to compare gasping of WT with that of knockout (KO) mice (see Results). The response, which followed periods of tachypnea (onset, open arrowhead in A2) and the initial depression (onset, filled arrow in A2), consisted of irregularly mixed depression (filled arrowheads in A2) and apnea-like periods (open squares in A2) frequently accompanying large body movement [extraordinarily large deflections in the piezoelectric transducer (PZT) trace in A1]. A stable, slow rhythm then emerged [inset (1)] and persisted until terminal breaths [inset (3), thin arrow]. During this slow rhythm, the PZT shape (lower trace in the insets) showed characteristics of either biphasic [inset (1)] or triphasic [asterisks in parentheses in inset (2)] persistent gasping. During the terminal breaths, a PZT shape characteristic of terminal gasping is seen [inset (3), thin arrow]. The polarity of the PZT deflection is affected by the posture of the mouse. Note that changes in percentage CO_2 correlated well with those of PZT responses. As a change in posture caused fluctuations in the response time of the percentage CO_2, CO_2 traces in the insets (above traces) were arranged to be readily correlated to individual PZT deflections. (B1 and B2) Similar to A but of a KO mouse subjected to 5.0% O_2. The hypoxic responses were irregular and persisted for only a short period. Filled arrowheads in insets (1) and (2) denote depression. Thin arrow in inset (3) denotes a terminal gasp showing an atypical PZT shape. Traces of respiratory frequency were discontinuous at some points due to large spontaneous body movements masking the breath.

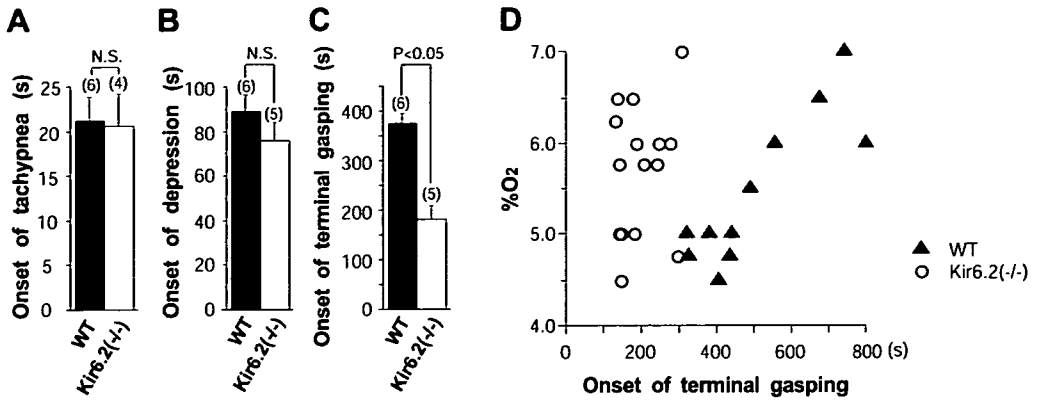

FIG. 12. Quantitative comparison of respiratory responses during hypoxia of wild-type (WT) and knockout (KO) mice in unanesthetized condition. (A–C) Comparison of onset of tachypnea, initial depression and terminal gasping, respectively, for very severe hypoxia (4.5–5.0% O_2). No significant difference was detected in the onset of tachypnea. The onset of the initial depression of KO mice was similar to that of WT mice. In contrast, terminal gasping of WT mice began significantly later than that of KO mice, demonstrating long duration of hypoxic response including depression, apnea and gasping in WT mice. (D) Onset of terminal gasping plotted against percentage O_2 (4.5–7.0%). The gasping onset of WT mice shortened linearly as the O_2 concentration was lowered, whereas those in KO mice were unaltered regardless of the concentrations within the range. Onset was measured from the time that the O_2 concentration began to decrease. N.S., not significant.

critical importance of central regulation in the maintenance of severe hypoxia-induced gasping.

Regarding the control of hypoxic gasping, the K_{ATP} channels in peripheral chemoreceptors such as the carotid body could also be involved. However, this is unlikely as the pattern of gasping and the magnitude of phrenic bursts during gasping are not altered by carotid sinus nerve stimulation (Neubauer *et al.*, 1990). In addition, initiation of gasping is not affected by sympathetic or parasympathetic blockade, such as intracarotid administration of NaCN, indicating a central regulation mechanism independent of autonomic integrity (St. John & Knuth, 1981; Sanocka *et al.*, 1992). Indeed, Kir6.2 mRNA was not detected in the carotid body of mice, although Kir6.1 mRNA was abundantly detected (data not shown).

Influence of CO_2 on gasping

Although gasping in the present study could result from hypocapnia rather than hypoxia, this is unlikely as neither the frequency nor the intensity of gasps was reported to be altered by hypocapnia (St. John & Knuth, 1981). In addition, it is known that phrenic nerve activity during gasping is not altered by reducing the end-tidal partial pressure of CO_2 from normocapnic to various hypocapnic levels (St. John & Knuth, 1981). Other investigators have also reported that the pattern of gasping and the magnitude of phrenic bursts during gasping are not altered by hypercapnea (Neubauer *et al.*, 1990). Indeed, in our experiment, the difference in gasping between KO and wild-type mice under isocapnic hypoxia by 92% N_2/3% CO_2/5% O_2 was similar to that detected by 95% N_2/5% O_2 (data not shown).

Hypoxia-induced sighs and apnea-like period

In the initial hypoxic period under anesthetized condition, both wild-type and KO mice showed similar onset and numbers of sighs, indicating that Kir6.2-containing K_{ATP} channels are not required for the initiation or maintenance of sighs, although their involvement in the modification of rhythmicity or relative amplitude cannot be excluded.

Regarding the apnea-like period between sighs following tachypnea in KO mice, no such period was detected in wild-type mice under anesthetized condition. In addition, it is noted that very fast breathing-like motions could be detected by PZT during a portion of the apnea-like period.

In unanesthetized condition, apnea (Fig. 11, A2) was detected not only in KO but also in wild-type mice in the middle stage of hypoxia. It is thus of interest to determine if the very fast breathing-like motions occur during apnea in the conscious state, and whether this is related to the similar peak period of tachypnea and onset of depression observed in both types of mice in unanesthetized condition.

Definition of gasping in mice

Among the conventionally used criteria of gasping, the rapid rise-time of integrated phrenic bursts is reported to be inappropriate in small mammals such as mice for distinguishing gasping from eupnea (Fukuda, 2000; St. John & Paton, 2003). In the present study, we included data on expiratory activity detected by PZT and divided gasping in the anesthetized condition in adult mice into persistent gasping of biphasic PZT shape and terminal gasping of wide phrenic bursts. Discrimination of the period of persistent gasping from that of depression was based on the symmetry and stability of the PZT shape, which reflects the balance between inspiratory and expiratory body movement detected by the vertical motion of the PZT.

In addition, gasping shown by triphasic shape was detected in the unanesthetized condition. Distinct types of gasping have also been reported by Gozal *et al.* (1996) with whole body plethysmography of immature rats in an alert condition. Prolonged, severe hypoxia elicited a triphasic ventilation consisting of an initial expiration followed by an inspiration and a second expiration (type I gasps), and a biphasic ventilation consisting of a prominent initial inspiration followed by a small expiration (type II gasps) (Gozal *et al.*, 1996). In their study, no biphasic gasping of symmetrical shape corresponding to persistent gasping was mentioned. The relationship between triphasic and biphasic gasping, and how expiration contributes to gasping are also of interest.

Mechanism of gasping

The cellular mechanisms underlying eupnea and gasping have been discussed extensively (Ramirez *et al.*, 1998; Koshiya & Smith, 1999; Lieske *et al.*, 2000; Del Negro *et al.*, 2002; Ramirez & Lieske, 2003; St. John & Paton, 2003; Pena *et al.*, 2004; Paton *et al.*, 2006). It is

proposed that gasping depends on intrinsic cellular mechanisms localized in the pre-Botzinger complex in the medulla, especially persistent sodium channel-dependent cellular properties (Del Negro *et al.*, 2002; Pena *et al.*, 2004; Paton *et al.*, 2006), whereas eupnea depends on the complex interaction of neuronal networks in the brainstem, either restricted or not restricted to the pre-Botzinger complex. Selective lesioning of the pre-Botzinger complex eliminates eupneic breathing but not gasping (Ramirez *et al.*, 1998), suggesting a complex nature of gasping *in vivo*. It has been reported that K_{ATP} channels comprising Kir6.2/SUR1 but not Kir6.1/SUR2 are expressed in inspiratory neurons in the pre-Botzinger complex by single-cell antisense RNA amplification-polymerase chain reaction (Haller *et al.*, 2001). Thus, it is of interest to clarify the participation of K_{ATP} channels in the regulation of hypoxic ventilatory responses.

The present results using KO mice lacking Kir6.2 indicate that these K_{ATP} channels are not essential for generating eupnea, sighs and gasping but rather are critically involved in maintaining a level of gasping and depression proportionate to the severity of the hypoxia, which might well be essential in recovery by reoxygenation (Neubauer *et al.*, 1990). In addition, of the hypoxia-induced ventilatory responses, only gasping and depression but not sigh were critically affected in KO mice, suggesting an alternative mechanism of control of sighs. The combination of recordings of phrenic nerve activity and PZT responses in spontaneously breathing animals highlights the importance of expiratory as well as inspiratory patterns in classifying depression and gasping.

It is proposed that the duration of survival of neurons in the respiratory centres after decapitation is determined by the balance between the anoxic energy reserve and the cerebral metabolic rate (Thurston *et al.*, 1978). Opening of the K_{ATP} channels, which couple the intracellular metabolic state with electrical activity, could well minimize energy consumption to protect the brain in such conditions (Ballanyi, 2004; Yamada & Inagaki, 2005). Further investigation is required to clarify how K_{ATP} channels participate in the central regulation of depression and gasping under severe hypoxia.

Supplementary material

The following supplementary material may be found on www.blackwell-synergy.com

Fig. S1. Typical changes in respiration of wild-type and knockout mice subjected to hypoxia without anesthesia.

Acknowledgements

This work was supported by Grant-in-aid for Scientific Research (15590181), JSPS Fellows (1650112), and Creative Scientific Research (15GS0301) from the Ministry of Education, Culture, Sports, Science and Technology of Japan. We are grateful to Drs Shinichi Sato, Masanori Nakata, Ya-Juan Zheng, Katsuaki Yoshizaki, Ms Kana Kato and Ms Emiko Harada (Akita University) for technical help.

Abbreviations

K_{ATP} channel, ATP-sensitive potassium channel; KO, knockout; PZT, piezo-electric transducer; SUR, sulfonylurea receptor.

References

Ashcroft, F.M. (1988) Adenosine 5′-triphosphate-sensitive potassium channels. *Annu. Rev. Neurosci.*, **11**, 97–118.

Ballanyi, K. (2004) Protective role of neuronal K_{ATP} channels in brain hypoxia. *J. Exp. Biol.*, **207**, 3201–3212.

Del Negro, C.A., Morgado-Valle, C. & Feldman, J.L. (2002) Respiratory rhythm: an emergent network property? *Neuron*, **34**, 821–830.

Fazekas, J.F., Alexander, F.A.D. & Himwich, H.E. (1941) Tolerance of the newborn to anoxia. *Am. J. Physiol.*, **134**, 281–287.

Fewell, J.E. (2005) Protective responses of the newborn to hypoxia. *Resp. Physiol. Neurobiol.*, **149**, 243–255.

Fukuda, Y. (2000) Respiratory neural activity responses to chemical stimuli in newborn rats: reversible transition from normal to 'secondary' rhythm during asphyxia and its implication for 'respiratory like' activity of isolated medullary preparation. *Neurosci. Res.*, **38**, 407–417.

Gang, S., Sato, Y., Kohama, I. & Aoki, M. (1995) Afferent projections to the Botzinger complex from the upper cervical cord and other respiratory related structures in the brainstem in cats: retrograde WGA-HRP tracing. *J. Auton. Nerv. Syst.*, **56**, 1–7.

Gozal, D., Torres, J.E., Gozal, Y.M. & Nuckton, T.J. (1996) Characterization and developmental aspects of anoxia-induced gasping in the rat. *Biol. Neonate*, **70**, 280–288.

Haller, M., Mironov, S.L., Karschin, A. & Richter, D.W. (2001) Dynamic activation of K_{ATP} channels in rhythmically active neurons. *J. Physiol. (Lond.)*, **537**, 69–81.

Holowach-Thurston, J., Hauhart, R.E. & Jones, E.M. (1974) Anoxia in mice: reduced glucose in brain with normal or elevated glucose in plasma and increased survival after glucose treatment. *Pediat. Res.*, **8**, 238–243.

Inagaki, N., Gonoi, T., Clement, J.P., Namba, N., Inazawa, J., Gonzalez, G., Aguilar-Bryan, L., Seino, S. & Bryan, J. (1995) Reconstitution of IKATP: An inward rectifier subunit plus the sulfonylurea receptor. *Science*, **270**, 1166–1170.

Inagaki, N., Gonoi, T., Clement, J.P., Wang, C.Z., Aguilar-Bryan, L., Bryan, J. & Seino, S. (1996) A family of sulfonylurea receptors determines the pharmacological properties of ATP-sensitive K^+ channels. *Neuron*, **16**, 1011–1017.

Khurana, A. & Thach, B.T. (1996) Effects of upper airway stimulation on swallowing, gasping, and autoresuscitation in hypoxic mice. *J. Appl. Physiol.*, **80**, 472–477.

Koshiya, N. & Smith, J.C. (1999) Neuronal pacemaker for breathing visualized in vitro. *Nature*, **400**, 360–363.

Lieske, S.P., Thoby-Brisson, M., Telgkamp, P. & Ramirez, J.M. (2000) Reconfiguration of the neural network controlling multiple breathing patterns: eupnea, sighs and gasps. *Nat. Neurosci.*, **3**, 600–607.

Miki, T., Nagashima, K., Tashiro, F., Kotake, K., Yoshitomi, H., Tamamoto, A., Gonoi, T., Iwanaga, T., Miyazaki, J. & Seino, S. (1998) Defective insulin secretion and enhanced insulin action in K_{ATP} channel-deficient mice. *Proc. Natl Acad. Sci. U.S.A.*, **95**, 10 402–10 406.

Miki, T., Suzuki, M., Shibasaki, T., Uemura, H., Sato, T., Yamaguchi, K., Koseki, H., Iwanaga, T., Nakaya, H. & Seino, S. (2002) Mouse model of prinzmetal angina by disruption of the inward rectifier Kir6.1. *Nat. Med.*, **8**, 466–472.

Miller, J.A. (1949) Factors of neonatal resistance to anoxia. I. Temperature and survival of guinea pigs under anoxia. *Science*, **110**, 113–114.

Mironov, S.L., Langohr, K., Haller, M. & Richter, D.W. (1998) Hypoxia activates ATP-dependent potassium channels in inspiratory neurones of neonatal mice. *J. Physiol. (Lond.)*, **509**, 755–766.

Mourre, C., Ben Ari, Y., Bernardi, H., Fosset, M. & Lazdunski, M. (1989) Antidiabetic sulfonylureas: localization of binding sites in the brain and effects on the hyperpolarization induced by anoxia in hippocampal slices. *Brain Res.*, **486**, 159–164.

Nakamura, A., Fukuda, Y. & Kuwaki, T. (2003) Sleep apnea and effect of chemostimulation on breathing instability in mice. *J. Appl. Physiol.*, **94**, 525–532.

Neubauer, J.A., Melton, J.E. & Edelman, N.H. (1990) Modulation of respiration during brain hypoxia. *J. Appl. Physiol.*, **68**, 441–451.

Noma, A. (1983) ATP-regulated K+ channels in cardiac muscle. *Nature*, **305**, 147–148.

Paton, J.F.R., Abdala, A.P.L., Koizumi, H., Smith, J.C. & St. John, W.M. (2006) Respiratory rhythm generation during gasping depends on persistent sodium current. *Nat. Neurosci.*, **9**, 311–313.

Pena, F., Parkis, M.A., Tryba, A.K. & Ramirez, J.M. (2004) Differential contribution of Pacemaker properties to the generation of respiratory rhythms during normoxia and hypoxia. *Neuron*, **43**, 105–117.

Ramirez, J.M. & Lieske, S.P. (2003) Commentary on the definition of eupnea and gasping. *Resp. Physiol. Neurobiol.*, **139**, 113–119.

Ramirez, J.M., Schwarzacher, S.W., Pierrefiche, O., Olivera, B.M. & Richter, D.W. (1998) Selective lesioning of the cat pre-Botzinger complex in vivo eliminates breathing but not gasping. *J. Physiol. (Lond.)*, **507**, 895–907.

Sanocka, U.M., Donnelly, D.F. & Haddad, G.G. (1992) Autoresuscitation: a survival mechanism in piglets. *J. Appl. Physiol.*, **73**, 749–753.

Sato, S., Yamada, K. & Inagaki, N. (2006) System for simultaneously monitoring heart and breathing rate in mice using a piezoelectric transducer. *Med. Biol. Eng. Comput.*, **44**, 353–362.

Secher, O. & Wilhjelm, B. (1968) The protective action of anesthetics against hypoxia. *Can. Anaes. Soc. J.*, **15**, 423–440.

Seino, S. (1999) ATP-sensitive potassium channels: a model of heteromultimeric potassium channel/receptor assemblies. *Annu. Rev. Physiol.*, **61**, 337–362.

Selle, W.A. (1944) Influence of glucose on the gasping pattern of young animals subjected to acute anoxia. *Am. J. Physiol.*, **141**, 297–302.

Selle, W.A. & Witten, T.A. (1941) Survival of the respiratory (gasping) mechanism in young animals subjected to anoxia. *Proc. Soc. Exp. Biol. Med.*, **47**, 495–497.

St. John, W.M. & Knuth, K.V. (1981) A characterization of the respiratory pattern of gasping. *J. Appl. Physiol.*, **50**, 984–993.

St. John, W.M. & Paton, J.F.R. (2003) Defining eupnea. *Respir. Physiol. Neurobiol.*, **139**, 97–103.

Thurston, J.H., Hauhard, R.E. & Dirgo, J.A. (1978) Aminophylline increases cerebral metabolic rate and decreases anoxic survival in young mice. *Science*, **201**, 649–651.

Wang, W., Fung, M.L., Darnall, R.A. & St. John, W.M. (1996) Characterizations and comparisons of eupnoea and gasping in neonatal rats. *J. Physiol. (Lond.)*, **490**, 277–292.

Yamada, K. & Inagaki, N. (2005) Neuroprotection by K_{ATP} channels. *J. Mol. Cell. Cardiol.*, **38**, 945–949.

Yamada, K., Ji, J.J., Yuan, H., Miki, T., Sato, S., Horimoto, N., Shimizu, T., Seino, S. & Inagaki, N. (2001) Protective role of ATP-sensitive potassium channels in hypoxia-induced generalized seizure. *Science*, **292**, 1543–1546.

DIABETES RESEARCH AND CLINICAL PRACTICE XXX (2008) XXX–XXX

available at www.sciencedirect.com

ScienceDirect

journal homepage: www.elsevier.com/locate/diabres

International Diabetes Federation

Curcumin inhibits glucose production in isolated mice hepatocytes

Hideya Fujiwara [a], *Masaya Hosokawa* [a,*], *Xiaorong Zhou* [a], *Shimpei Fujimoto* [a], *Kazuhito Fukuda* [a], *Kentaro Toyoda* [a], *Yuichi Nishi* [a], *Yoshihito Fujita* [a], *Kotaro Yamada* [a], *Yuichiro Yamada* [a], *Yutaka Seino* [a,b], *Nobuya Inagaki* [a]

[a] *Department of Diabetes and Clinical Nutrition, Graduate School of Medicine, Kyoto University, 54 Shogoin, Kawahara-cho, Sakyo-ku, Kyoto 606-8507, Japan*

[b] *Kansai Denryoku Hospital, Osaka, Japan*

ARTICLE INFO

Article history:
Received 18 October 2007
Accepted 6 December 2007

Keywords:
Curcumin
Diabetes mellitus
Liver
Mice

ABSTRACT

Curcumin is a compound derived from the spice turmeric, and is a potent anti-oxidant, anti-carcinogenic, and anti-hepatotoxic agent. We have investigated the acute effects of curcumin on hepatic glucose production. Gluconeogenesis and glycogenolysis in isolated hepatocytes, and gluconeogenetic enzyme activity after 120 min exposure to curcumin were measured. Hepatic gluconeogenesis from 1 mM pyruvate was inhibited in a concentration-dependent manner, with a maximal decrease of 45% at the concentration of 25 μM. After 120 min exposure to 25 μM curcumin, hepatic gluconeogenesis from 2 mM dihydroxyacetone phosphate and hepatic glycogenolysis were inhibited by 35% and 20%, respectively. Insulin also inhibited hepatic gluconeogenesis from 1 mM pyruvate and inhibited hepatic glycogenolysis in a concentration-dependent manner. Curcumin (25 μM) showed an additive inhibitory effect with insulin on both hepatic gluconeogenesis and glycogenolysis, indicating that curcumin inhibits hepatic glucose production in an insulin-independent manner. After 120 min exposure to 25 μM curcumin, hepatic glucose-6-phosphatase (G6Pase) activity and phosphoenolpyruvate carboxykinase (PEPCK) activity both were inhibited by 30%, but fructose-1,6-bisphosphatase (FBPase) was not reduced. After 120 min exposure to 25 μM curcumin, phosphorylation of AMP kinase α-Thr^{172} was increased. Thus, the anti-diabetic effects of curcumin are partly due to a reduction in hepatic glucose production caused by activation of AMP kinase and inhibition of G6Pase activity and PEPCK activity.

1. Introduction

Curcumin is the major yellow pigment extracted from turmeric, the powdered rhizome of the herb *curcuma longa*. Turmeric is a spice used extensively in curries and mustards as a coloring and flavoring agent. Curcumin is reported to have a wide range of effects: it is anti-inflammatory [1], anti-oxidant [2,3] anti-hepatotoxic [4], and hypocholesterolemic [5,6]. Curcumin also is reported to have a beneficial effect on blood glucose in diabetic rats [7,8]. However, while elevated hepatic glucose production is

* *Corresponding author.* Tel.: +81 75 751 3560; fax: +81 75 751 4244.
E-mail address: hosokawa@metab.kuhp.kyoto-u.ac.jp (M. Hosokawa).

Abbreviations: DHAP, dihydroxyacetone phosphate; FBP, fructose-1,6-bisphophatase; G6Pase, glucose-6-phosphatase; PEPCK, phosphoenolpyruvate carboxykinase; AMP kinase, adenosine monophosphate activated protein kinase.

0168-8227/$ – see front matter © 2007 Elsevier Ireland Ltd. All rights reserved.
doi:10.1016/j.diabres.2007.12.004

Please cite this article in press as: H. Fujiwara et al., Curcumin inhibits glucose production in isolated mice hepatocytes, Diab. Res. Clin. Pract. (2008), doi:10.1016/j.diabres.2007.12.004

found frequently in type 2 diabetes, it is not known whether curcumin affects glucose metabolism in the liver. In the present study, we demonstrate that curcumin suppresses hepatic glucose production in an insulin-independent manner in isolated hepatocytes. We also investigated the inhibitory effect of curcumin on the activity of gluconeogenetic enzymes in isolated hepatocytes. Our results show that curcumin activates AMP kinase and suppresses both hepatic glucose-6-phosphatase (G6Pase) and phosphoenolpyruvate carboxykinase (PEPCK), thus inhibiting hepatic glucose output.

2. Materials and methods

2.1. Animals

C57/BL6J mice were purchased from Shimizu (Kyoto, Japan). The mice were allowed access to food, standard rat chow (Oriental Yeast, Osaka, Japan), and water *ad lib*. The mice were housed in an air-controlled (temperature 25 ± 2 °C and 50% humidity) room with a 12 h light/dark-cycle. For gluconeogenesis measurements, the mice were fasted 24 h with free access to water before the experiment. For glycogenolysis measurements, the mice were allowed access to food and water *ad lib* before the experiment.

2.2. Hepatocyte preparation

Liver of 10-week-old mice was perfused through the inferior *vena cava* with a buffer consisting of 140 mM NaCl, 2.6 mM KCl, 0.28 mM Na_2HPO_4, 5 mM glucose, and 10 mM Hepes (pH 7.4) after pentobarbital sodium anesthesia as described previously in Refs. [9,10]. The perfusion was first for 5 min with the buffer supplemented with 0.1 mM EGTA and then for 15 min with the buffer containing 5 mM $CaCl_2$ and 0.2 mg/ml collagenase type 2 (Worthington, Lakewood, NJ). All of the solutions were prewarmed at 37 °C and gassed with a mixture of 95% O_2/5%CO_2, resulting in pH 7.4. The isolated hepatocytes were filtered with nylon mesh (0.75 mm in diameter) and washed twice with the buffer above without collagenase, and suspended in a small volume of DMEM (GIBCO, Rockville, MD) without glucose or pyruvate, and counted. The viability of hepatocytes was evaluated by trypan blue staining. Samples with viability of less than 90% were discarded.

2.3. Hepatic glucose production

For gluconeogenesis measurements, hepatocytes (7.5×10^5) were incubated at 37 °C in a humidified atmosphere (5% CO_2) in 0.5 ml of DMEM without glucose but containing 1 mM pyruvate or 2 mM dihydroxyacetone phosphate (DHAP), 0.24 mM 3-isobutyl-1-methylxanthine in the presence or absence of curcumin or insulin. For glycogenolysis measurements, hepatocytes (7.5×10^5) were incubated at 37 °C in a humidified atmosphere (5% CO_2) in 0.5 ml of DMEM without glucose or pyruvate but containing 0.24 mM 3-isobutyl-1-methylxanthine in the presence or absence of curcumin or insulin. Curcumin was dissolved in DMSO to a concentration in the medium that did not interfere with cell viability (maximally 0.1%, v/v). Incubation was stopped by placing the cells on ice, followed by centrifugation at 4 °C for 60 s at 600 × *g*. The sampling was done at 0, 30, 60, and 120 min. The supernatant was removed, the cells were lysed in 0.1% of SDS in phosphate buffered saline, and the protein content was determined (BCA kit, Pierce). The glucose content of the supernatant was measured by glucose oxidation method (100 Trinder kit, Sigma). The dose–response of curcumin in gluconeogenesis and glycogenolysis were obtained at the incubation time of 120 min.

2.4. DNA synthesis measurement

DNA synthesis of hepatocytes was determined as the uptake of 5-bromo-2′-deoxyuridine (BrdU) according to the instruction manual (Cell Proliferation ELISA, BrdU (colorimetric), Roche Diagnostics, Manheim, Germany). After a 24-h preincubation of isolated hepatocytes with curcumin (25 μM) or vehicle in DMEM without glucose but with 10% fetal calf serum, hepatocytes were incubated for an additional 2 h with BrdU. The hepatocytes were fixed, and BrdU incorporation into DNA in hepatocytes was detected by ELISA. The results of incorporation of BrdU were expressed as photo-absorbance (wavelength 370–492 nm).

2.5. Enzyme activities

Hepatocytes were incubated at 37 °C in a humidified atmosphere (5% CO_2) in DMEM without glucose but containing 1 mM pyruvate and 0.24 mM 3-isobutyl-1-methylxanthine in the presence of 25 μM curcumin or vehicle (DMSO) for 120 min. Incubation was stopped by placing the cells on ice followed by centrifugation at 4 °C for 60 s at 600 × *g*. The supernatant was removed, and the cells were homogenized using a glass/Teflon homogenizer. In the microsomal preparation for the G6Pase assay, 50 mM Tris–HCl, pH 7.5, containing 250 mM sucrose, and 0.2 mM EDTA, was used as the homogenizing buffer [11]. For assay of G6Pase, liver microsomal fraction was prepared as follows: homogenate obtained as above was centrifuged at 20,000 × *g* for 20 min at 4 °C, and was then ultracentrifuged at 105,000 × *g* for 1 h at 4 °C. The resulting sediments were used for G6Pase assay [11]. The G6Pase activity was measured with intact microsomal preparation. Activity of G6Pase was determined as described by Passonneau and Lowry [12].

For liver PEPCK and fructose-1,6-bisphophatase (FBPase) assays, the homogenizing buffer contained 0.1 M Tris–HCl, pH 7.5, 0.15 M KCl, 5 mM EDTA, 5 mM dithiothreitol, and 5 mM $MgSO_4$ [11]. The homogenate was centrifuged at 105,000 × *g* for 1 h at 4 °C, and the supernatant was collected. Activity of FBPase was determined as described by Passonneau and Lowry [12].

Activity of PEPCK was determined as described by Nakagawa and Nagai [13]. All enzyme activity was measured photometrically using BIO-RAD Benchmark Plus.

Enzyme activities are expressed as the number of substrate molecules converted by 1 mg cytosolic or microsomal protein per minute. The liver microsomal fraction was solubilized by addition of 0.1% SDS before protein determination.

2.6. Immunoblotting analysis

Hepatocytes were incubated at 37 °C in a humidified atmosphere (5% CO_2) in 10 ml of DMEM without glucose but

Please cite this article in press as: H. Fujiwara et al., Curcumin inhibits glucose production in isolated mice hepatocytes, Diab. Res. Clin. Pract. (2008), doi:10.1016/j.diabres.2007.12.004

containing 1 mM pyruvate and 0.24 mM 3-isobutyl-1-methylxanthine in the presence of 25 μM curcumin or vehicle (DMSO) for 120 min. Incubation was stopped by placing the cells on ice followed by centrifugation at 4 °C for 60 s at 600 × *g*. The supernatant was removed, and the cells were homogenized in ice-cold lysis buffer (50 mM Tris–HCl, pH 7.4, 50 mM NaF, 1 mM sodium pyrophosphate, 1 mM EDTA, 1 mM EGTA, 1 mM dithiothreitol, 0.1 mM benzamidine, 0.1 mM phenylmethylsulfonylfluoride, 0.2 mM sodium vanadate, 250 mM mannitol, 1% Triton X-100, and 5 μg/ml soybean trypsin inhibitor). The cell lysates were sonicated twice for 10 s and centrifuged at 13,000 × *g* for 5 min. The pellets were discarded, and supernatants were assayed for protein concentration. Equal amounts of proteins (50 μg) were subjected to SDS-polyacrylamide (8%) gel electrophoresis and transferred onto nitrocellulose membranes (PROTRAN, Schleicher & Schuell) by electroblotting. After pre-incubation with blocking buffer (PBS containing 0.1% Tween 20 and 5% nonfat dry milk) for 2 h at room temperature, blotted membranes were incubated with each primary antibody (phospho-AMP kinase α-Thr^{172} antibody or AMP kinase α antibody, Cell Signaling Technology, Danvers, MA) overnight at 4 °C, followed by washing twice with blocking buffer. Membranes were then incubated with a horseradish peroxidase-linked anti-rabbit IgG (Amersham) for 1 h at room temperature, washed twice in PBS containing 0.04% Tween 20, and visualized by ECL Western blotting detection reagents (Amersham). Densitometry was carried out to measure band intensities and phosphorylated AMP kinase α-Thr^{172} was normalized by the levels of AMP kinase α protein.

2.7. Materials

Curcumin was purchased from Wako Chemicals (Osaka, Japan). Standard rat chow was from Oriental Yeast (Osaka, Japan). Human insulin was from Novo-Nordisk (Copenhagen, Denmark). All other chemicals were of reagent grade.

2.8. Statistical analysis

Results are mean ± S.E.M. (*n* = number of animals). Statistical significance was evaluated using two-tailed Student's t-tests. Differences among groups were also statistically examined by one-way ANOVA (Fisher's PLSD test). $P < 0.05$ was considered significant.

2.9. Ethical considerations

All studies were performed in the laboratories of the Department of Diabetes and Clinical Nutrition, Kyoto University, in accordance with the Declaration of Helsinki.

3. Results

3.1. Effect of curcumin on hepatic gluconeogenesis in freshly isolated hepatocytes

Fig. 1A shows the time course of inhibition by curcumin of hepatic gluconeogenesis from pyruvate. After 30, 60, and 120 min exposure to 25 μM curcumin, hepatic gluconeogenesis was significantly inhibited by approximately 45%, 40%, and 45%, respectively. The viability of the hepatocytes was not affected by 120 min exposure to 25 μM curcumin (control: 78 ± 1% vs. curcumin: 79 ± 2%). Fig. 1B shows the time course of inhibition by curcumin of hepatic gluconeogenesis from dihydroxyacetone phosphate. After 120 min exposure to 25 μM curcumin, hepatic gluconeogenesis was significantly inhibited by approximately 35%.

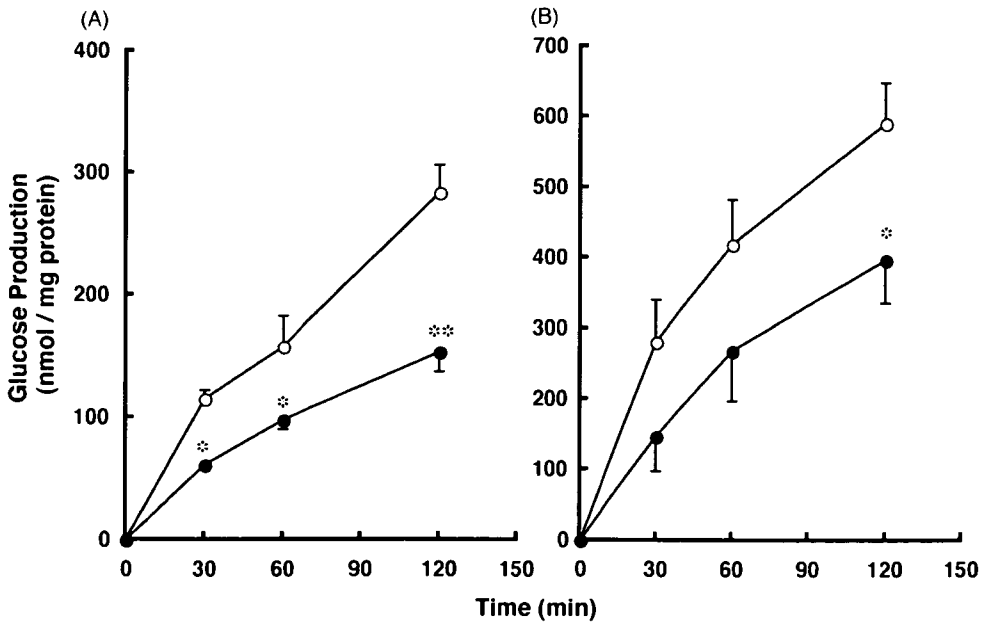

Fig. 1 – Time course of inhibition in hepatic gluconeogenesis from 1 mM pyruvate (A) and 2 mM DHAP (B). Isolated hepatocytes from fasted mice were incubated in the presence of 25 μM curcumin or vehicle for 2 h. Glucose content in supernatant was measured by glucose oxidation method. Each point shows mean ± S.E.M. (*n* = 6). *P < 0.05, **P < 0.01 compared with control by unpaired Student's t-test. Control (○), curcumin (●).

Please cite this article in press as: H. Fujiwara et al., Curcumin inhibits glucose production in isolated mice hepatocytes, Diab. Res. Clin. Pract. (2008), doi:10.1016/j.diabres.2007.12.004

As shown in Fig. 2, curcumin inhibited hepatic gluconeogenesis from pyruvate at the incubation time of 120 min in a concentration-dependent manner.

As shown in Fig. 3, after 120 min exposure to insulin, hepatic gluconeogenesis from pyruvate was inhibited in a concentration-dependent manner. After 120 min exposure to various concentrations of insulin (0.1, 1, and 10 nM) in the presence of 25 μM curcumin, hepatic gluconeogenesis from pyruvate was further inhibited by approximately 45% when compared to that in the absence of 25 μM curcumin.

3.2. *Effect of curcumin on DNA synthesis in isolated hepatocytes*

To determine whether curcumin is toxic to hepatocytes, we examined the effect of curcumin on DNA synthesis in isolated hepatocytes. After 24 h exposure to 25 μM curcumin, BrdU incorporation into DNA in isolated hepatocytes was not decreased compared to control, indicating no suppressive effects of curcumin on DNA synthesis (Fig. 4).

3.3. *Effect of curcumin on hepatic glycogenolysis in freshly isolated hepatocytes*

Fig. 5A shows the time course of inhibition by curcumin of hepatic glucose production from glycogenolysis. After 60 and 120 min exposure to 25 μM curcumin, hepatic glycogenolysis was significantly inhibited by approximately 10% and 20%, respectively. As shown in Fig. 5B, curcumin inhibited hepatic glycogenolysis at the incubation time of 120 min in a concentration-dependent manner. As shown in Fig. 6, after

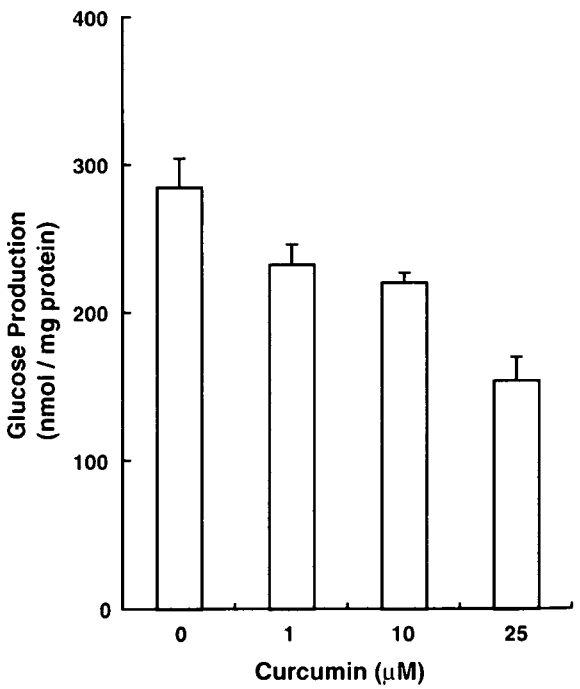

Fig. 2 – Concentration-dependence of inhibition in gluconeogenesis from 1 mM pyruvate by curcumin at the incubation time of 120 min in isolated mice hepatocytes. Each point shows mean ± S.E.M. ($n = 6$). $P < 0.001$ by one-way ANOVA.

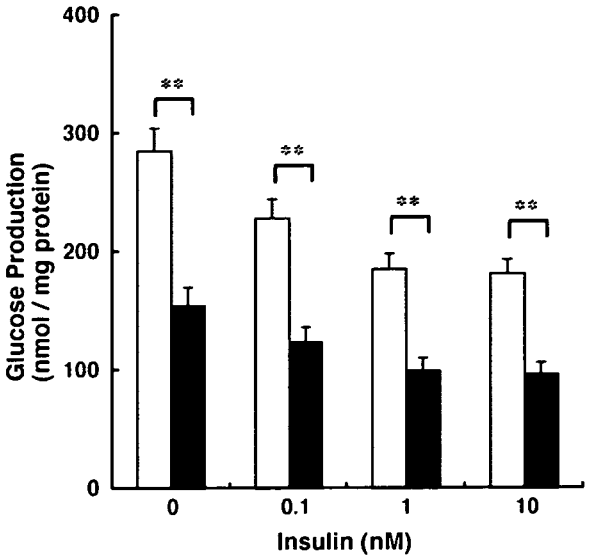

Fig. 3 – Concentration-dependence of inhibition in gluconeogenesis from 1 mM pyruvate by insulin in the presence and absence of 25 μM curcumin in isolated mice hepatocytes. Each point shows mean ± S.E.M. ($n = 6$). $P < 0.001$ by one-way ANOVA. **$P < 0.01$ compared with insulin alone by unpaired Student's t-test. Insulin alone (open bar), insulin plus curcumin (closed bar).

120 min exposure to insulin, hepatic glycogenolysis was inhibited in a concentration-dependent manner. After 120 min exposure to various concentrations of insulin (0.1, 1, and 10 nM) in the presence of 25 μM curcumin, hepatic glycogenolysis was further inhibited by approximately 20% compared to that in the absence of 25 μM curcumin.

3.4. *Effect of curcumin on activities of hepatic gluconeogenetic enzymes*

To further investigate inhibition of hepatic glucose production by curcumin, we measured the activities of key gluconeogenetic enzymes, G6Pase, FBPase, and PEPCK. After 120 min exposure to 25 μM curcumin, hepatic G6Pase activity and PEPCK activity were significantly inhibited by approximately 30%, but FBPase was not inhibited (Fig. 7).

3.5. *Effect of curcumin on phosphorylation of AMP kinase*

AMP kinase activation was monitored in Western blots by staining with a specific antibody against phosphorylated Thr^{172} of AMP kinase α, which is essential for AMP kinase activity. After 120 min exposure to 25 μM curcumin, phosphorylation of AMP kinase α-Thr^{172} was significantly increased by 70% when normalized by total content of AMP kinase α, clearly indicating curcumin activation of AMP kinase (Fig. 8).

4. Discussion

This is the first study to show that curcumin reduces hepatic glucose production. Our results demonstrate that curcumin

Please cite this article in press as: H. Fujiwara et al., Curcumin inhibits glucose production in isolated mice hepatocytes, Diab. Res. Clin. Pract. (2008), doi:10.1016/j.diabres.2007.12.004

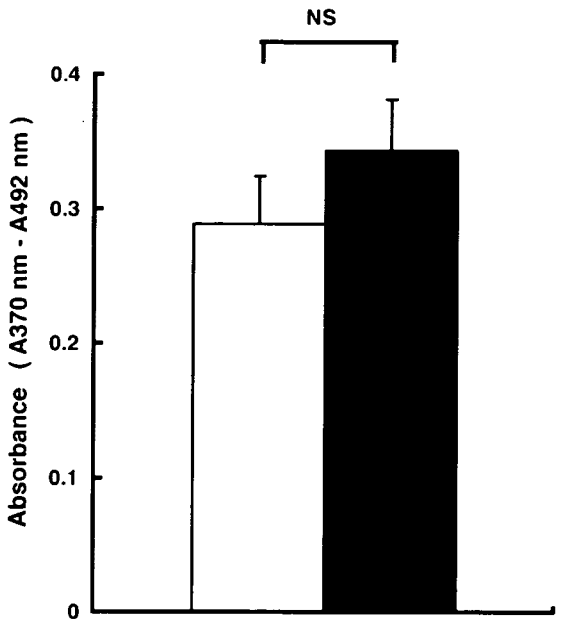

Fig. 4 – The effect of curcumin on DNA synthesis in isolated hepatocytes. After 24-h pre-incubation of isolated mice hepatocytes with 25 μM curcumin or vehicle in DMEM without glucose but with 10% fetal calf serum, hepatocytes were incubated for an additional 2 h with BrdU. The results of incorporation of BrdU were expressed as photo-absorbance (wavelength 370–492 nm). Control (open bar), curcumin (closed bar).

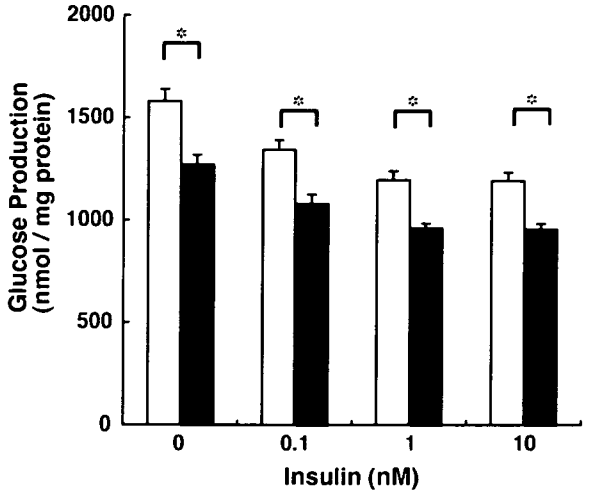

Fig. 6 – Concentration-dependence of inhibition in glycogenolysis by insulin in the presence and absence of 25 μM curcumin at the incubation time of 120 min in isolated mice hepatocytes. Each point shows mean ± S.E.M. ($n = 6$). $P < 0.001$ by one-way ANOVA. *$P < 0.05$ compared with insulin alone by unpaired Student's t-test. Insulin alone (open bar), insulin plus curcumin (closed bar).

inhibits both hepatic gluconeogenesis and glycogenolysis by suppressing both G6Pase activity and PEPCK activity. As curcumin had no suppressive effect on DNA synthesis in isolated hepatocytes, the inhibition of hepatic glucose production should not be a toxic effect. Indeed, Shen et al.

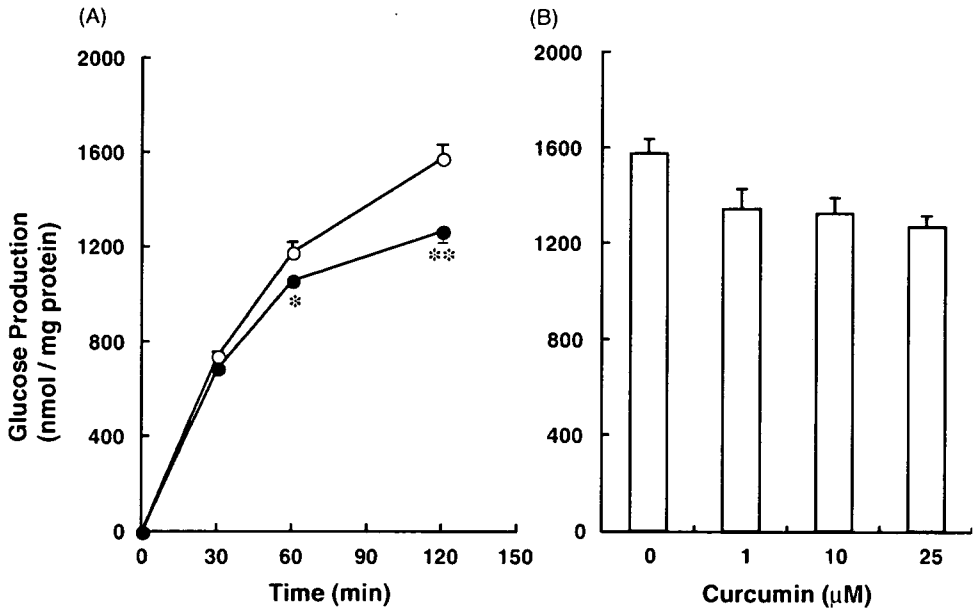

Fig. 5 – (A) Time course of inhibition of hepatic glucose production from glycogenolysis by curcumin. Isolated hepatocytes from fed mice were incubated in the presence of 25 μM curcumin or vehicle for 2 h. Glucose content in supernatant was measured by glucose oxidation method. Each point shows mean ± S.E.M. ($n = 5$). *$P < 0.05$, **$P < 0.01$ compared with control by unpaired Student's t-test. Control (○), curcumin (●). (B) Concentration-dependence of inhibition of glycogenolysis by curcumin at the incubation time of 120 min in isolated mice hepatocytes. Each point shows mean ± S.E.M. ($n = 6$). $P < 0.05$ by one-way ANOVA.

Please cite this article in press as: H. Fujiwara et al., Curcumin inhibits glucose production in isolated mice hepatocytes, Diab. Res. Clin. Pract. (2008), doi:10.1016/j.diabres.2007.12.004

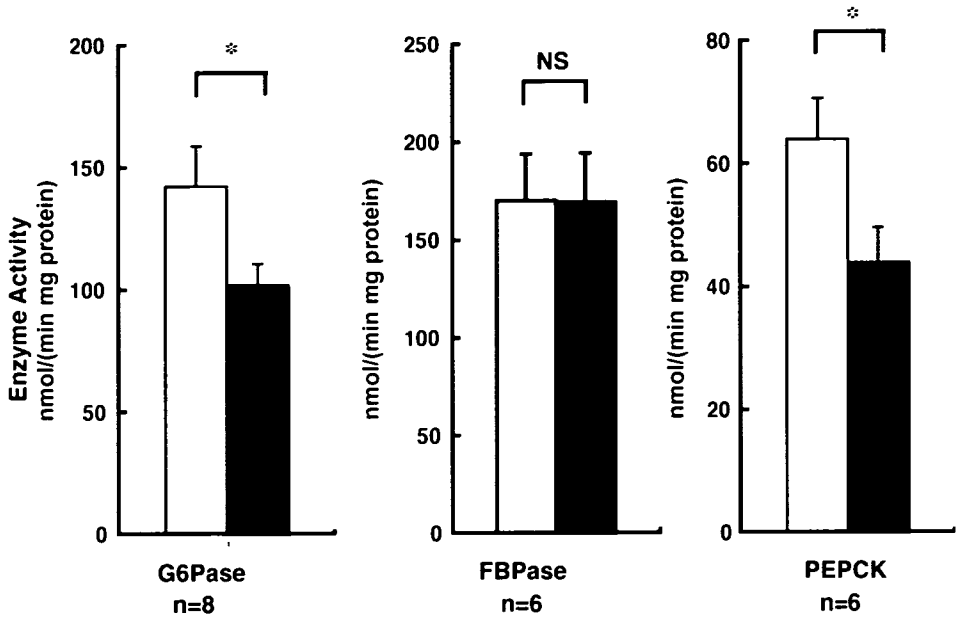

Fig. 7 – Effects of curcumin on hepatic gluconeogenetic activities of G6Pase, FBPase, and PEPCK in isolated mice hepatocyte. Isolated hepatocytes from fasted mice were incubated in the presence of 25 μM curcumin or vehicle for 2 h. All enzyme activities were measured photometrically. Enzyme activities are expressed as the number of substrate molecules converted by 1 mg cytosolic or microsomal protein per minute. Each point shows mean ± S.E.M. *P < 0.05 compared with control by unpaired Student's t-test. Control (open bar), curcumin (closed bar).

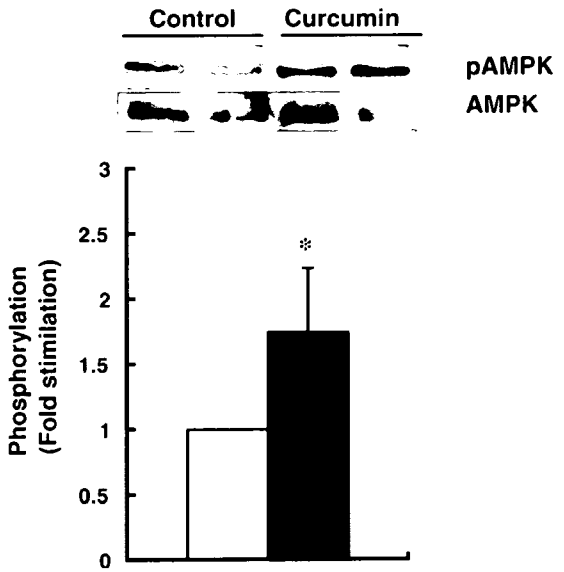

Fig. 8 – Effect of curcumin on activation of AMP kinase in isolated mice hepatocytes. AMP kinase activation was monitored in Western blots by staining with a specific antibody against phosphorylated Thr^{172} of AMP kinase α. After 120 min exposure to 25 μM curcumin, the level of phosphorylation of AMP kinase α-Thr^{172} (pAMPK) was significantly increased by 70% when normalized by total content of AMP kinase α (AMPK), and is expressed as fold stimulation over the control (mean ± S.E.M., n = 5) (lower panel). Upper panel shows a representative immunoblot of pAMPK and AMPK in hepatocytes from two mice in each group. *P < 0.05 compared with control by unpaired Student's t-test. Control (open bar), curcumin (closed bar).

recently reported a protective effect of curcumin against warm ischemia/reperfusion injury in rat liver [14].

Arun and Nalini reported that curcumin reduced blood glucose in alloxan-induced diabetic rats [7], but the mechanism of the anti-diabetic action was left unclear in that study. In the present study, insulin was found to dose-dependently inhibit hepatic gluconeogenesis, reaching a plateau at a concentration of 10 nM. In the presence of 10 nM insulin, the addition of 25 μM curcumin enchanced the inhibitory effect of insulin on hepatic gluconeogenesis, demonstrating that curcumin inhibits hepatic gluconeogenesis by a pathway independent of insulin signaling. Thus, curcumin is an insulin-sentitizing agent.

Recently, the major effect of metformin, a biguanide, was reported to be inhibition of hepatic G6Pase activity and hepatic glucose production in rats fed a high-fat diet [15]. Zhou et al. reported that metformin activated AMP kinase in hepatocytes [16]. The activation of AMP kinase is known to suppress gene expression of G6Pase and PEPCK and to inhibit hepatic glucose production in an insulin-independent manner [17,18]. In the present study, curcumin was found to inhibit both G6Pase and PEPCK activity; we therefore measured the effect of curcumin on AMP kinase activity to clarify the underlying mechanism. Zang et al. reported that resveratrol, a polyphenol and an anti-oxidant, which is a key component in red wine, stimulates AMP kinase in hepatoma HepG2 cells [19]. Kim et al. reported that cryptotanshinone, another anti-oxidant and a diterpene, which was originally isolated from dried roots of *Salvia mlitorrhiza* Bunge, showed anti-diabetic effects through activation of AMP kinase [20]. Considering these findings together, the potent anti-oxidant effect of curcumin may

Please cite this article in press as: H. Fujiwara et al., Curcumin inhibits glucose production in isolated mice hepatocytes, Diab. Res. Clin. Pract. (2008), doi:10.1016/j.diabres.2007.12.004

well be involved in the activation of AMP kinase. Further investigation is required to clarify the anti-diabetic action of curcumin in hepatocytes.

Biguanide sometimes shows the lethal adverse effect of lactic acidosis in diabetic patients when prescribed inappropriately. On the other hand, since curcumin is derived from an extensively used dietary spice, the compound may well be safely administered to humans. Indeed, Sharma et al. administered oral daily curcumin to advanced colorectal cancer patients without major adverse effects [21]. Cheng et al. also administered oral daily curcumin to patients with high risk or pre-malignant lesions [22].

Considered together with our results, these data suggest that curcumin might provide a valuable new therapy in the treatment of type 2 diabetes.

Acknowledgements

This study was supported in part by Grants-in-Aids for Scientific Research from the Ministry of Education, Culture, Sports, Science and Technology of Japan; Health and Labour Sciences Research Grants for Research on Human Genome, Tissue Engineering, and Food Biotechnology from the Ministry of Health, Labor and Welfare of Japan; and Health and Labour Sciences Research Grants for Comprehensive Research on Aging and Health from the Ministry of Health, Labor and Welfare of Japan.

Conflict of interest

The authors state that they have no conflict of interest.

REFERENCES

[1] R.C. Srimal, B.N. Dhawan, Pharmacology of diferuloyl methane (curcumin), a non-steroidal anti-inflammatory agent, J. Pharm. Pharmacol. 25 (1973) 447–452.

[2] B. Joe, B.R. Lokesh, Role of capsaicin, curcumin and dietary n-3 fatty acids in lowering the generation of reactive oxygen species in rat peritoneal macrophages, Biochim. Biophys. Acta 1224 (1994) 255–263.

[3] A.C. Reddy, B.R. Lokesh, Studies on the inhibitory effects of curcumin and eugenol on the formation of reactive oxygen species and the oxidation of ferrous iron, Mol. Cell. Biochem. 137 (1994) 1–8.

[4] Y. Kiso, Y. Suzuki, N. Watanabe, Y. Oshima, H. Hikino, Antihepatotoxic principles of *Curcuma longa* rhizomes, Planta Med. 49 (1983) 185–187.

[5] D.S. Rao, N.C. Sekhara, M.N. Satyanarayana, M. Srinivasan, Effect of curcumin on serum and liver cholesterol levels in the rat, J. Nutr. 100 (1970) 1307–1315.

[6] T.N. Patil, M. Srinivasan, Hypocholesteremic effect of curcumin in induced hypercholesteremic rats, Indian J. Exp. Biol. 9 (1971) 167–169.

[7] N. Arun, N. Nalini, Efficacy of turmeric on blood sugar and polyol pathway in diabetic albino rats, Plant Foods Hum. Nutr. 57 (2002) 41–52.

[8] T. Nishiyama, T. Mae, H. Kishida, M. Tsukagawa, Y. Mimaki, M. Kuroda, et al., Curcuminoids and sesquiterpenoids in turmeric (*Curcuma longa* L.) suppress an increase in blood glucose level in type 2 diabetic KK-Ay mice, J. Agric. Food Chem. 53 (2005) 959–963.

[9] M. Hosokawa, B. Thorens, Glucose release from GLUT2-null hepatocytes: characterization of a major and a minor pathway, Am. J. Physiol. Endocrinol. Metab. 282 (2002) E794–E801.

[10] M. Uldry, M. Ibberson, M. Hosokawa, B. Thorens, GLUT2 is a high affinity glucosamine transporter, FEBS Lett. 524 (2002) 199–203.

[11] K. Aoki, T. Saito, S. Satoh, K. Mukasa, M. Kaneshiro, S. Kawasaki, et al., Dehydroepiandrosterone suppresses the elevated hepatic glucose-6-phosphatase and fructose-1,6-bisphosphatase activities in C57BL/Ksj-db/db mice: comparison with troglitazone, Diabetes 48 (1999) 1579–1585.

[12] J.V. Passoneau, O.H. Lowry, Enzymic Analysis: A Practical Guide by Passoneau JV and Lowry OH., Humana Press, Totowa, NJ, 1993, pp. 249–253.

[13] H. Nakagawa, K. Nagai, Cold adaptation. I. Effect of cold-exposure on gluconeogenesis, J. Biochem. (Tokyo) 69 (1971) 923–934.

[14] S.Q. Shen, Y. Zhang, J.J. Xiang, C.L. Xiong, Protective effect of curcumin against liver warm ischemia/reperfusion injury in rat model is associated with regulation of heat shock protein and antioxidant enzymes, World J. Gastroenterol. 13 (2007) 1953–1961.

[15] G. Mithieux, L. Guignot, J.C. Bordet, N. Wiernsperger, Intrahepatic mechanisms underlying the effect of metformin in decreasing basal glucose production in rats fed a high-fat diet, Diabetes 51 (2002) 139–143.

[16] G. Zhou, R. Myers, Y. Li, Y. Chen, X. Shen, J. Fenyk-Melody, et al., Role of AMP-activated protein kinase in mechanism of metformin action, J. Clin. Invest. 108 (2001) 1167–1174.

[17] P.A. Lochhead, I.P. Salt, K.S. Walker, D.G. Hardie, C. Sutherland, 5-Aminoimidazole-4-carboxamide riboside mimics the effects of insulin on the expression of the 2 key gluconeogenic genes PEPCK and glucose-6-phosphatase, Diabetes 49 (2000) 896–903.

[18] T. Yamauchi, J. Kamon, Y. Minokoshi, Y. Ito, H. Waki, S. Uchida, et al., Adiponectin stimulates glucose utilization and fatty-acid oxidation by activating AMP-activated protein kinase, Nat. Med. 8 (2002) 1288–1295.

[19] M. Zang, S. Xu, K.A. Maitland-Toolan, A. Zuccollo, X. Hou, B. Jiang, et al., Polyphenols stimulate AMP-activated protein kinase, lower lipids, and inhibit accelerated atherosclerosis in diabetic LDL receptor-deficient mice, Diabetes 55 (2006) 2180–2191.

[20] E.J. Kim, S.N. Jung, K.H. Son, S.R. Kim, T.Y. Ha, M.G. Park, et al., Antidiabetes and antiobesity effect of cryptotanshinone via activation of AMP-activated protein kinase, Mol. Pharmacol. 72 (2007) 62–72.

[21] R.A. Sharma, S.A. Euden, S.L. Platton, D.N. Cooke, A. Shafayat, H.R. Hewitt, et al., Phase I clinical trial of oral curcumin: biomarkers of systemic activity and compliance, Clin. Cancer Res. 10 (2004) 6847–6854.

[22] A.L. Cheng, C.H. Hsu, J.K. Lin, M.M. Hsu, Y.F. Ho, T.S. Shen, et al., Phase I clinical trial of curcumin, a chemopreventive agent, in patients with high-risk or pre-malignant lesions, Anticancer Res. 21 (2001) 2895–2900.

Please cite this article in press as: H. Fujiwara et al., Curcumin inhibits glucose production in isolated mice hepatocytes, Diab. Res. Clin. Pract. (2008), doi:10.1016/j.diabres.2007.12.004

Comparison of M-Kyoto Solution and Histidine–Tryptophan–Ketoglutarate Solution With a Trypsin Inhibitor for Pancreas Preservation in Islet Transplantation

Hirofumi Noguchi,[1,2,3,4,6] Michiko Ueda,[3] Shuji Hayashi,[2] Naoya Kobayashi,[5] Hideo Nagata,[3] Yasuhiro Iwanaga,[1] Teru Okitsu,[1] and Shinichi Matsumoto[3,4]

The use of University of Wisconsin (UW) preservation solution in islet transplantation has some disadvantages, including inhibition of collagenase activity for pancreatic digestion. Histidine–tryptophan–ketoglutarate (HTK) solution has demonstrated an efficacy similar to UW solution for organ preservation in clinical pancreas transplantation. Recently, we reported that islet yield from porcine pancreata was significantly gtreater when they were preserved using M-Kyoto solution compared with UW solution. Here, we compared HTK solution with ulinastatin (M-HTK) and M-Kyoto solution for islet yield. In porcine islet isolation, islet yield after purification was significantly greater in the M-Kyoto/perfluorochemical (PFC) group compared with the M-HTK/PFC group. The M-Kyoto/PFC group had a significantly lower ADP/ATP ratio compared with the M-HTK/PFC group, suggesting that different islet yields might be due to the differences as energy sources of the solutions used. In conclusion, M-Kyoto/PFC solution is better for pancreas preservation before islet isolation than M-HTK/PFC solution.

Keywords: Islet transplantation, Islet isolation, M-Kyoto solution, Histidine–tryptophan–ketoglutarate solution, Trypsin inhibitor.

(*Transplantation* 2007;84: 655–658)

Pancreatic islet transplantation represents a viable option for the treatment of patients with unstable type 1 diabetes mellitus who have frequent severe hypoglycemia and hypoglycemia unawareness (*1–6*). Since the Edmonton protocol was announced, more than 500 type 1 diabetes patients in more than 50 institutions have undergone islet transplantation to cure their disease. However, treatment of diabetic patients by pancreatic islet transplantation often requires the use of islets from two to four donors to produce insulin independence in a single recipient (*1, 2, 5, 6*). After isolation and transplantation, islets are susceptible to apoptosis, which limits their function and probably long-term islet graft survival.

Donor pancreata usually are preserved with University of Wisconsin (UW) solution. Recent reports have shown that the two-layer method (TLM), which uses oxygenated perfluorochemical (PFC) and UW solution, is superior to simple cold storage in UW not only for preserving the whole pancreas but also for improved viable islet yield in subsequent islet transplantation (*7, 8*). However, use of UW solution in islet transplantation has some disadvantages. The high potassium concentration in UW solution causes insulin release from pancreatic β cells (*9*), and the high viscosity of UW solution may prevent sufficient flushing. Moreover, UW solution inhibits the activity of Liberase, an enzyme blend used for pancreatic digestion (*10, 11*). Our previous study showed that ET-Kyoto (Kyoto solution®, Otsuka Pharmaceutical, Tokyo, Japan) with ulinastatin (Miraclid®, Mochida Pharmaceutical, Tokyo, Japan) (M-Kyoto) in combination with PFC significantly improved viable islet yields compared with UW/PFC preservation (*12*). The effectiveness of ET-Kyoto solution has also been demonstrated in clinical lung transplantation (*13, 14*) and skin flap storage (*15*). ET-Kyoto solution contains trehalose and gluconate. Trehalose has a cytoprotective effect against stress, and gluconate acts as an extracellular anti-oncotic agent, which prevents cells from swelling (*16*). Histidine–tryptophan–ketoglutarate (HTK) solution (Custodiol®, Alsbach, Hähnlein, Germany), originally developed for cardioplegia, is being used with increasing frequency in cardiac, renal, and hepatic transplantation (*17, 18*). The protective effect of HTK solution is based on the strong buffering capacity of histidine. This solution has a low viscosity, easy handling properties and a relatively low cost. Some studies have demonstrated comparable results between UW and HTK solution for pancreas preservation not only in experimental animal models (*19–21*) but also clinical pancreas transplantation (*22–24*).

In this study, we compared M-Kyoto solution with HTK solution containing ulinastatin (M-HTK) for islet isolation. Animal studies were approved by the Institu-

Supported in part by the Ministry of Education, Science and Culture, the Ministry of Health, Labor and Welfare.

[1] Transplantation Unit, Kyoto University Hospital, Shogoin, Sakyo-ku, Kyoto, Japan.
[2] Department of Advanced Medicine in Biotechnology and Robotics, Nagoya University Graduate School of Medicine, Showa-ku, Nagoya, Japan.
[3] Fujita Health University, Second Department of Surgery, Kutsukake-cho, Toyoake, Aichi, Japan.
[4] Baylor Institute for Immunology Research, Baylor Research Institute, Dallas, TX.
[5] Department of Surgery, Okayama University Graduate School of Medicine and Dentistry, Okayama, Japan.
[6] Address correspondence to: Hirofumi Noguchi, M.D., Ph.D., Baylor Institute for Immunology Research, Baylor Research Institute, 3434 Live Oak St., Dallas, TX 75204.
E-mail: hirofumn@baylorhealth.edu

Received 10 May 2007. Revision requested 31 May 2007.
Accepted 31 May 2007.

ISSN 0041-1337/07/8405-655
DOI: 10.1097/01.tp.0000277625.42147.62

TABLE 1. Pig islet isolation characteristics

	M-Kyoto (n=6)	M-HTK (n=4)
Pancreas size (g)	105.2±17.8	108.9±29.0
Operation time (min)	7.8±2.1	7.0±2.2
Warm ischemic time (min)	26.7±3.6	26.0±2.9
Cold ischemic time (min)	123.0±3.5	123.5±3.1
Phase I period (min)	10.2±3.6	9.5±2.1
Phase II period (min)	35.3±6.1	32.8±8.6

Data are expressed as mean±SD.

TABLE 2. Pig islet characteristics

	M-Kyoto (n=6)	M-HTK (n=4)
Islet yield before purification (IE/g)	10,121±1,674	7,904±4,970
Islet yield after purification (IE/g)[a]	6,599±1,854	3,147±1,979
Viability (%)	96.5±2.7	96.4±4.4
Score	9.3±0.6	9.5±1.0
Purity (%)	70.0±16.7	82.2±21.9
Recovery rate (%)	65.6±17.9	43.4±13.3
Stimulation iIndex	2.29±0.67	1.58±0.23

Data are expressed as mean±SD.
[a] Islet yield after purification was significantly greater in the M-Kyoto/PFC group than in the M-HTK/PFC group ($P<0.05$).

tional Animal Research Committees of Kyoto University, Nagoya University, and Fujita Health University. Porcine pancreata were obtained at a local slaughterhouse. About 10 minutes after the cessation of heart beating, the surgery was started. After removing the pancreas, we immediately inserted a cannula into the main pancreatic duct, infused either M-Kyoto or M-HTK preservation solution for ductal protection, and placed the pancreas into the respective two-layer preservation container (M-Kyoto/PFC or M-HTK/PFC). Islet isolation was conducted in accordance with the Kyoto Islet Isolation Method modified in the Edmonton protocol (*1, 4–6, 8, 12*). The characteristics of the porcine islet isolation protocols are shown in Table 1. There were no significant differences in pancreas size, operation time, warm ischemic time, cold ischemic time, Phase I period, or Phase II period between the two groups. Islet yield before purification was higher, but not significantly so, in the M-Kyoto/PFC group (n=6) compared with the M-HTK/PFC group (n=4). Islet yield after purification was significantly higher in the M-Kyoto/PFC group compared with the M-HTK/PFC group (Table 2). Other porcine islet characteristics are shown in Table 2. There were no other significantly different characteristics between the two groups.

Islet function was assessed by the adenosine diphosphate (ADP)/adenosine triphosphate (ATP) ratio, which shows the energy status of islets and correlates with transplantation outcome, according to a procedure described by Goto and colleagues (*25*). The ADP/ATP ratio was measured using the ApoGlowTM kit (Cambrex Bio Science Nottingham Ltd., Nottingham, UK). The ADP/ATP ratio in the M-Kyoto/PFC group was significantly lower than in the M-HTK/PFC group (Fig. 1A). These data suggest that different islet isolation effects between the two preservation solutions might be due to their differences as energy sources. To assess the islet graft function of each group in vivo, mice with severe combined immunodeficiency disease (SCID; CLEA Japan, Inc., Meguro, Tokyo) were used for the experiments. The recipients were rendered diabetic by a single injection of streptozotocin (STZ) at a dose of 220 mg/kg. The 1,500 or 2,000 IE pig islets obtained from each group were transplanted into the renal subcapsular space of the left kidney of diabetic SCID mice as previously described (*26–28*). When 1500 IEs from each group were transplanted below the kidney capsule of STZ-induced diabetic SCID mice, the normoglycemic rate was

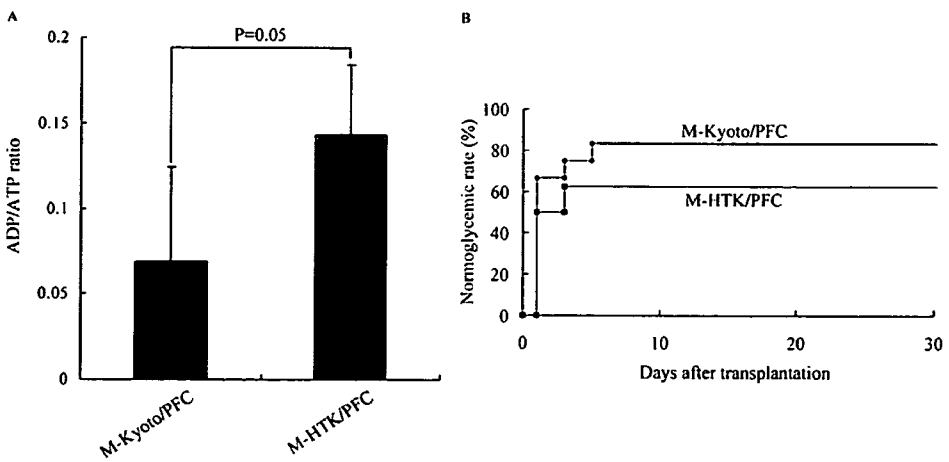

FIGURE 1. ADP/ATP ratio and transplant experiment. (A) The ADP/ATP ratio was measured to evaluate the energy status of cultured islets using the ApoGlowTM kit. The ADP/ATP ratio in the M-Kyoto/PFC group was barely lower than in the M-HTK/PFC group. Data are expressed as the mean±standard deviation. (B) Normoglycemic rate of STZ-induced diabetic SCID mice after islet transplantation. Immediately after isolation, 1,500 IEs were transplanted below the kidney capsule of diabetic SCID mice. Normoglycemia was defined as two consecutive posttransplant blood glucose levels showing less than 200 mg/dl (M-Kyoto group n=12; M-HTK group n=8).

greater, but not significantly so, in the M-Kyoto/PFC group (n=12) compared with the M-HTK/PFC group (n=8) (Fig. 1B). When 2000 IEs from each group were transplanted below the kidney capsule of STZ-induced diabetic SCID mice, the normoglycemic rate was more than 80% in both groups.

Inhibitory effects of collagenase on preservation solutions, such as UW solution, result in poor islet yield and islets of poor viability (*10, 11*). It has been reported that the components in UW solution found to be most inhibitory were magnesium, low Na+/high K+, hydroxyethyl starch (HES), and adenosine. Allopurinol, in combination with either lactobionate or glutathione, was markedly inhibitory, and the most inhibitory solution tested was a combination of three components, raffinose, glutathione, and lactobionate (*11*). M-Kyoto solution has high Na+/low K+ and, of the UW components, it contains only HES at a lower concentration. Moreover, trehalose and ulinastatin in M-Kyoto solution inhibit collagenase digestion less than UW solution (*12*). The M-HTK solution includes magnesium, but does not include HES, adenosine, allopurinol, lactobionate, glutathione, or raffinose. It has also been shown that the adenosine, allopurinol, and glutathione are not essential for the cold storage of pancreatic digests prior to islet purification (*29*). To assess the inhibitory effects on collagenase by M-Kyoto and M-HTK solutions, the rate of inhibition on collagenase digestion was measured in accordance with the modified method as previously described (*11*). The median digestion time was 79.0±2.9 min for M-Kyoto solution and 77.0±1.3 min for M-HTK solution. There are no significant differences between the two solutions on collagenase activity. Therefore, the different islet yields after purification are not due to differences in collagenase inhibition between these two solutions.

The TLM is important for preserving pancreata before islet isolation because it helps to preserve the organ, whereas UW preservation results in the deterioration of both islet isolation efficacy and posttransplant islet function (*7, 8*). The pancreas is directly oxygenated by PFC during pancreas preservation and maintains a high level of ATP in tissues. ATP drives a sodium pump, maintains cell integrity and repairs warm ischemic injury (*30, 31*). After significant warm ischemic injury, adenosine in UW solution is used as a substrate of ATP synthesis, however, without significant warm ischemia, ATP is generated from ADP or AMP located in the cells. We showed previously that ATP levels after preservation in M-Kyoto/PFC were similar to those in UW/PFC preservation and that adenosine is not importance for ATP generation when the warm ischemic time was less than thirty minutes (*12*). In this study, neither the M-Kyoto solution nor the M-HTK solution included adenosine. The ADP/ATP ratio in the M-Kyoto/PFC group was around half of that measured in the M-HTK/PFC group (Fig. 1), suggesting that different islet isolation effects between the two preservation solutions might be because of their differences as energy sources. Because energy status is an excellent predictor of successful pancreas transplantation (*32*), a low ADP/ATP ratio also might reflect effective two-layer preservation. Gluconate as an energy source or trehalose as a cytoprotectant might contribute to the effective M-Kyoto/PFC preservation of warm ischemically damaged pancreata.

In conclusion, M-Kyoto solution is superior to M-HTK solution for islet isolation. The improved pancreas preservation and islet isolation by M-Kyoto solution was not due to differences in collagenase digestion between the two solutions. However, a significantly lower ADP/ATP ratio was observed in the M-Kyoto/PFC group, compared to the M-HTK/PFC group, suggesting that the energy sources might be a factor in the islet yield differences observed between the two solutions. On the basis of these data, we now use M-Kyoto solution for clinical islet transplantation from non-heart-beating donor (NHBD) pancreata. M-Kyoto/PFC preservation makes it feasible to use NHBDs for efficient islet transplantation into type 1 diabetes.

ACKNOWLEDGMENTS

The authors thank Mr. Yusuke Nakai (Kyoto University), Dr. Xiaoling Liu, and Hiroki Kamiya (Fujita Health University) for technical support; Dr. Carson Harrod for editing the manuscript; and Ms. Nobuyo Hatanaka and Maki Watanabe (Fujita Health University) for assistance.

REFERENCES

1. Shapiro AM, Lakey JR, Ryan EA, et al. Islet transplantation in seven patients with type 1 diabetes mellitus using a glucocorticoid-free immunosuppressive regimen. *N Engl J Med* 2000; 343: 230.
2. Froud T, Ricordi C, Baidal DA, et al. Islet transplantation in type 1 diabetes mellitus using cultured islets and steroid-free immunosuppression: Miami experience. *Am J Transplant* 2005; 5: 2037.
3. Hering BJ, Kandaswamy R, Ansite JD, et al. Single-donor, marginal-dose islet transplantation in patients with type 1 diabetes. *JAMA* 2005; 293: 830.
4. Matsumoto S, Okitsu T, Iwanaga Y, et al. Insulin independence after living-donor distal pancreatectomy and islet allotransplantation. *Lancet* 2005; 365: 1642.
5. Noguchi H, Iwanaga Y, Okitsu T, et al. Evaluation of islet transplantation from non-heart beating donors. *Am J Transplant* 2006; 6: 2476.
6. Matsumoto S, Okitsu T, Iwanaga Y, et al. Successful islet transplantation from nonheartbeating donor pancreata using modified Ricordi islet isolation method. *Transplantation* 2006; 82: 460.
7. Matsumoto S, Kuroda Y. Perfluorocarbon for organ preservation before transplantation. *Transplantation* 2002; 74: 1804.
8. Matsumoto S, Qualley SA, Goel S, et al. Effect of the two-layer (University of Wisconsin solution-perfluorochemical plus O2) method of pancreas preservation on human islet isolation, as assessed by the Edmonton Isolation Protocol. *Transplantation* 2002; 74: 1414.
9. Fujimoto S, Mukai E, Hamamoto Y, et al. Prior exposure to high glucose augments depolarization-induced insulin release by mitigating the decline of ATP level in rat islets. *Endocrinology* 2002; 143: 213.
10. Robertson GS, Chadwick D, Thirdborough S, et al. Human islet isolation—a prospective randomized comparison of pancreatic vascular perfusion with hyperosmolar citrate or University of Wisconsin solution. *Transplantation* 1993; 56: 550.
11. Contractor HH, Johnson PR, Chadwick DR, et al. The effect of UW solution and its components on the collagenase digestion of human and porcine pancreas. *Cell Transplant* 1995; 4: 615.
12. Noguchi H, Ueda M, Nakai Y, et al. Modified two-layer preservation method (M-Kyoto/PFC) improves islet yields in islet isolation. *Am J Transplant* 2006; 6: 496.
13. Omasa M, Hasegawa S, Bando T, et al. Application of ET-Kyoto solution in clinical lung transplantation. *Ann Thorac Surg* 2004; 77: 338.
14. Chen F, Fukuse T, Hasegawa S, et al. Effective application of ET-Kyoto solution for clinical lung transplantation. *Transplant Proc* 2004; 36: 2812.
15. Wu SF, Suzuki Y, Kitahara AK, et al. Skin flap storage with intracellular and extracellular solutions containing trehalose. *Ann Plast Surg* 1999; 43: 289.
16. Belzer FO, Southard JH. Organ preservation and transplantation. *Prog Clin Biol Res* 1986; 224: 291.

17. Bretschneider HJ. Myocardial protection. *Thorac Cardiovasc Surg* 1980; 28: 295.
18. Erhard J, Lange R, Scherer R, et al. Comparison of histidine–tryptophan–ketoglutarate (HTK) solution versus University of Wisconsin (UW) solution for organ preservation in human liver transplantation. A prospective, randomized study. *Transpl Int* 1994;7: 177.
19. Hesse UJ, Troisi R, Jacobs B, et al. Cold preservation of the porcine pancreas with histidine–tryptophan–ketoglutarate solution. *Transplantation* 1998; 66: 1137.
20. Troisi R, Meester D, Van Den Broecke C, et al. Functional and structural integrity of porcine pancreatic grafts subjected to a period of warm ischemia and cold preservation with histidine–tryptophan–ketoglutarate (custodiol) or University of Wisconsin solution. Transplantation. 2003; 75: 1793.
21. Leonhardt U, Tytko A, Exner B, et al. The effect of different solutions for organ preservation on immediate postischemic pancreatic function in vitro. *Transplantation* 1993; 55: 11.
22. Potdar S, Malek S, Eghtesad B, et al. Initial experience using histidine–tryptophan–ketoglutarate solution in clinical pancreas transplantation. *Clin Transplant* 2004; 18: 661.
23. Englesbe MJ, Moyer A, Kim DY, et al. Early pancreas transplant outcomes with histidine–tryptophan–ketoglutarate preservation: A multicenter study. *Transplantation* 2006; 82: 136.
24. Fridell JA, Agarwal A, Milgrom ML, et al. Comparison of histidine–tryptophan–ketoglutarate solution and University of Wisconsin solution for organ preservation in clinical pancreas transplantation. *Transplantation* 2004; 77: 1304.
25. Goto M, Holgersson J, Kumagai-Braesch M, Korsgren O. The ADP/ATP ratio: A novel predictive assay for quality assessment of isolated pancreatic islets. *Am J Transplant* 2006; 6: 2483.
26. Noguchi H, Matsushita M, Okitsu T, et al. A new cell-permeable peptide allows successful allogeneic islet transplantation in mice. *Nat Med* 2004; 10: 305.
27. Noguchi H, Nakai Y, Matsumoto S, et al. Cell permeable peptide of JNK inhibitor prevents islet apoptosis immediately after isolation and improves islet graft function. *Am J Transplant* 2005; 5: 1848.
28. Noguchi H, Nakai Y, Ueda M, et al. Activation of c-Jun NH(2)-terminal kinase (JNK) pathway during islet transplantation and prevention of islet graft loss by intraportal injection of JNK inhibitor *Diabetologia* 2007; 50: 612.
29. Chadwick DR, Robertson GS, Contractor HH, et al. Storage of pancreatic digest before islet purification. The influence of colloids and the sodium to potassium ratio in University of Wisconsin-based preservation solutions. *Transplantation* 1994; 58: 99.
30. Matsumoto S, Fujino Y, Suzuki Y, et al. Evidence of protein synthesis during resuscitation of ischemically damaged canine pancreas by the two-layer method. *Pancreas* 2000; 20: 411.
31. Tanioka Y, Kuroda Y, Kim Y, et al. The effect of ouabain (inhibitor of an ATP-dependent Na+/K+ pump) on the pancreas graft during preservation by the two-layer method. *Transplantation* 1996; 62: 1730.
32. Morita A, Kuroda Y, Saitoh Y. Evaluation of the viability and energy metabolism of ischemically damaged canine pancreas during preservation by the two-layer (University of Wisconsin solution/perfluorochemical) cold storage method. *Kobe J Med Sci* 1992;38: 205.

Pancreas Development and β-Cell Differentiation of Embryonic Stem Cells

Jorge David Rivas-Carrillo[1], Teru Okitsu[2], Noriaki Tanaka[1] and Naoya Kobayashi*,[1]

[1]*Department of Surgery, Okayama University Graduate School of Medicine and Dentistry, 2-5-1 Shikata-cho, Okayama 700-8558, Japan*

[2]*Transplant Unit, Kyoto University Hospital, 54 Seigoin-Kawaracho, Sakyoku, Kyoto 606-8507, Japan*

Abstract: Embryonic stem (ES) cells may offer an unlimited cell source for the treatment of diabetes. However, a successful derivation of ES cells into islet-cells has proven to be more difficult than it was initially expected. Considering that the pancreas coordinates the global use of energy in the organism by secreting digestive enzymes and hormones, it is understandable that a sophisticated and tight regulation that lies on the pancreas itself to orchestrate its own tissue development and maturation. The complex process of endocrine cell differentiation can be better understood by analyzing the normal development of the pancreas. The proper detection of the signals provided in the pancreatic environment gives us a clue as to how the stem cells give rise to the whole pancreas. Careful and extensive screening of the natural or synthetic cytokines and growth factors and biochemical compounds that are essential in pancreatic development is required to properly mimic the process *in vitro*. Such a study would allow the researchers to achieve selective control of the differentiation and proliferation of the stem cells.

The development and identification of the key molecules can provide us new insights into the pancreatic differentiation of the stem cells. We herein discuss the role of the microenvironment and transcriptional factors and cytokines, which have been recognized as important molecules during the major steps of the development of the pancreas. Finally, a more complete comprehension of the mechanisms that drive the pancreatic regeneration will provide us with new perspectives for future prophylactic and therapeutic interventions.

Keywords: Pancreas development, β-cell differentiation, cell therapy, diabetes, stem cells, cell-fate modulation, tissue regeneration, tissue homeostasis.

INTRODUCTION

Clinical islet transplantation has been a very promising cure for diabetes mellitus, thus allowing patients to become insulin-independent using a glucocorticoid-free immunosuppressive regimen. However, given the current global donor shortage, the widespread use of islet transplantation has been seriously restricted [1, 2]. The generation of insulin-producing cells derived from embryonic stem (ES) cells could constitute a potential alternative source to the cadaveric-derived pancreatic islets for the treatment of diabetes. ES cells can be unlimitedly propagated *in vitro* while maintaining their undifferentiated state. ES cells are also able to closely mimic the natural development *in vitro* of forming spherical aggregates, the so-called embryoid bodies (EB). EB formation can itself derivate tissues of three germinal layers [3]. This early observation in EB has been widely used to differentiate islet cells. In addition, in order to remove the undesired cells and enrich the pancreatic committed cells population Insulin-Transferrin-sodium Selenium (ITS) selection has been widely utilized. The remaining cells are stimulated to grow and recover using growth factors such as epithelial growth factor (EGF) and fibroblast growth factor-2, (FGF-2) [4-7]. Eventually, such resulting cells after the intake of insulin can be artificially identified as insulin-secreting cells. However, these cells are actually incapable of synthesizing insulin de novo [6, 7]. These premature results have indicated that the difficulty in differentiating *bona-fide* the ES cells is greater than was that expected. Meanwhile, the natural development of the pancreas, which is tightly regulated by the local and neighboring stimuli, is poorly understood. We will herein mainly focus on the major steps of pancreatic development, which may contribute to a better understanding of the main factors involved in the β-cell differentiation process. Moreover, we will discuss the role of the major transcriptional factors, which drive the pancreatic islet development. Finally, this study may contribute to the development of new approaches for ES cell differentiation toward the β-cell phenotype.

ENDODERM FORMATION

ES cells are derived from the inner cell mass of the blastocyst; such ES cells are in fact a group of the undifferentiated cells localized in the epiblast. The epiblast-derived cells *in vivo* give rise to the three principal germ layers through a process called gastrulation, and thus their terminally differentiated tissues [3, 8]. The initiation of gastrulation is recognized by the formation of the primitive streak (PS) at the posterior part of the epiblast. Then, within the PS, the mesendoderm cells regulate the expression of several genes, such as goosecoid (GSC) forkhead box A2, (Foxa 2), chemokine C-X-C motif receptor 4 cxcr4, sex determining region-Y box 17 (Sox17α/β), brachyury, E-cadherin, vascular endothelial growth factor receptor-2, (VEGFR2), VE-cadherin, platelet-derived growth factor receptor-α (PDGFRα), and GATA binding protein 4, (GATA-4) for the cell-fate differentiation of the definitive endoderm and mesoderm progenitors. The endoderm has two main populations, namely the visceral and the definitive endoderm. The visceral endoderm is derived from the PS overlaying cells, which are eventually displaced to integrate with the extra-embryonic yolk sac related tissues [8, 9]. Such visceral yolk sacs can early and highly express α-fetoprotein, (AFP), albumin, insulin-II, and in a lower rate insulin-I too, but they lack Neurogenin-3 (Ngn3), Islet-1 (Isl-1), Neuro D/β2, and glucagon [10, 11]. Moreover, insulin-I, Neuro D/β2, and Isl-1 are expressed in both the endocrine cells and the neurons, but Ngn-3 and glucagon are exclusive to the endocrine- developing pancreas [12]. Therefore, insulin-, AFP- or albumin-analyses would not be appropriate. Contribution of the visceral yolk sac-derived cells and neurons can also overestimate the differentiated populations. In contrast, the definitive endoderm is only derived from within the PS, and mostly from the anterior part (Fig. **1**) [8, 9]. Recently, researchers have clearly demonstrated in a comprehensive study the *in vitro* differentiation of both human and mouse ES cells into the

*Address correspondence to this author at the Department of Surgery, Okayama University Graduate School of Medicine and Dentistry, 2-5-1 Shikata-cho, Okayama, 700-8558, Japan; Tel: (+81) 86-235-7485; Fax: (+81) 86-235-7485; E-mail: immortal@md.okayama-u.ac.jp

0929-8673/07 $50.00+.00

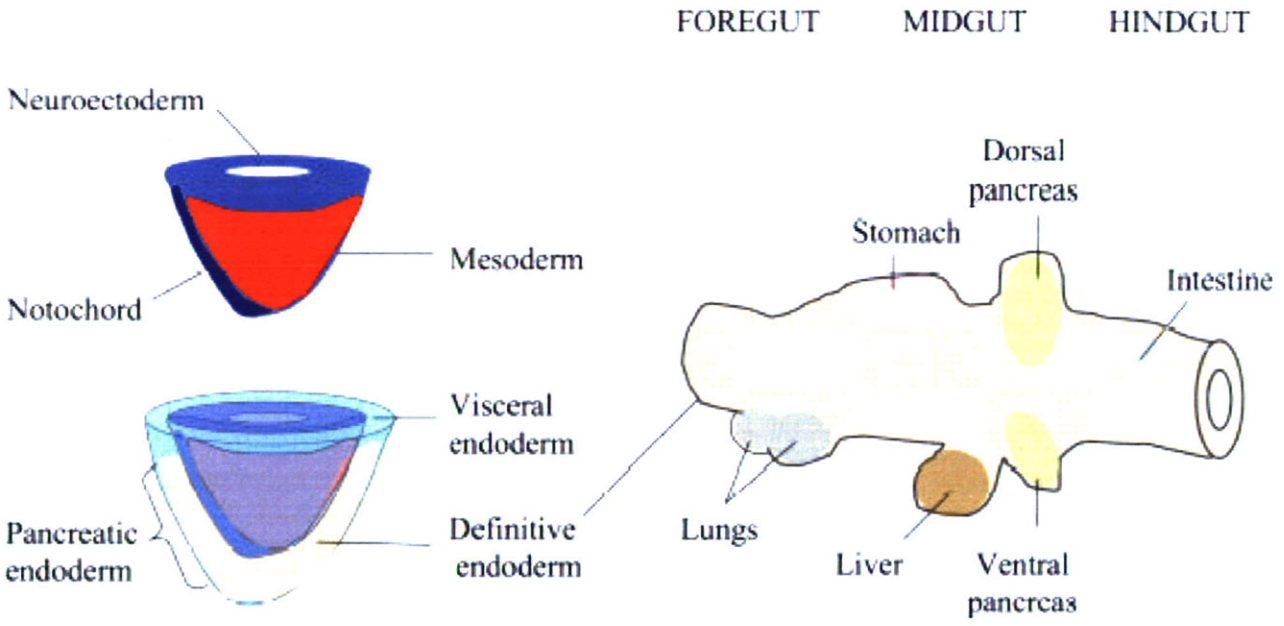

Fig. (1). Schematic representation of definitive endoderm and its derived tissues.

The *left panel* shows the normal distribution of the three germinal layers post-gastrulation and their relations, which determine the tissue-specific differentiation. The *right panel* shows how the definitive endoderm is responsible for deriving the entire gastrointestinal tract and lungs; in particular the portion subjacent to the notochord is capable of originating pancreatic tissue.

definitive endoderm with a high efficiency using Activin A and a low serum concentration. Their analyses clearly indicate the possibility to modulate *in vitro* a direct differentiation of the ES cells instead of the EB formation [9, 13]. The definitive endoderm cells are the only cells that can truly originate the gastrointestinal tract, including the pancreas and liver [9]. Researchers have found that the differentiation protocols based on EB formation can render less than 1% of the differentiated β-like cells. However, upon stimulation with Activin βB, Exendin-4, and nicotinamide, they may increase up to 2.73% [11]. Considering these results and the fact that the islet cells represent less than 2% of the total pancreatic tissue, different approaches are required.

DEVELOPMENT OF THE PRIMITIVE PANCREAS

Once committed, definitive endoderm cells align along the vertical body axis to form the gut tube, which is then divided into the foregut, midgut and hindgut. The dorsal primitive pancreas is derived from the dorsal endoderm of the foregut and midgut, along with the dorsal part of the esophagus, stomach, and duodenum (Fig. **1**). Initially, the dorsal endoderm and the notochord are united while flaked in the counterpart by the cardiogenic primordium until the dorsal aorta fuse (on E9.5 in mice), which separates the endoderm from the notochord. These extracellular signals from the neighboring cells result in the expression of the tissue- and cell type-specific transcriptional

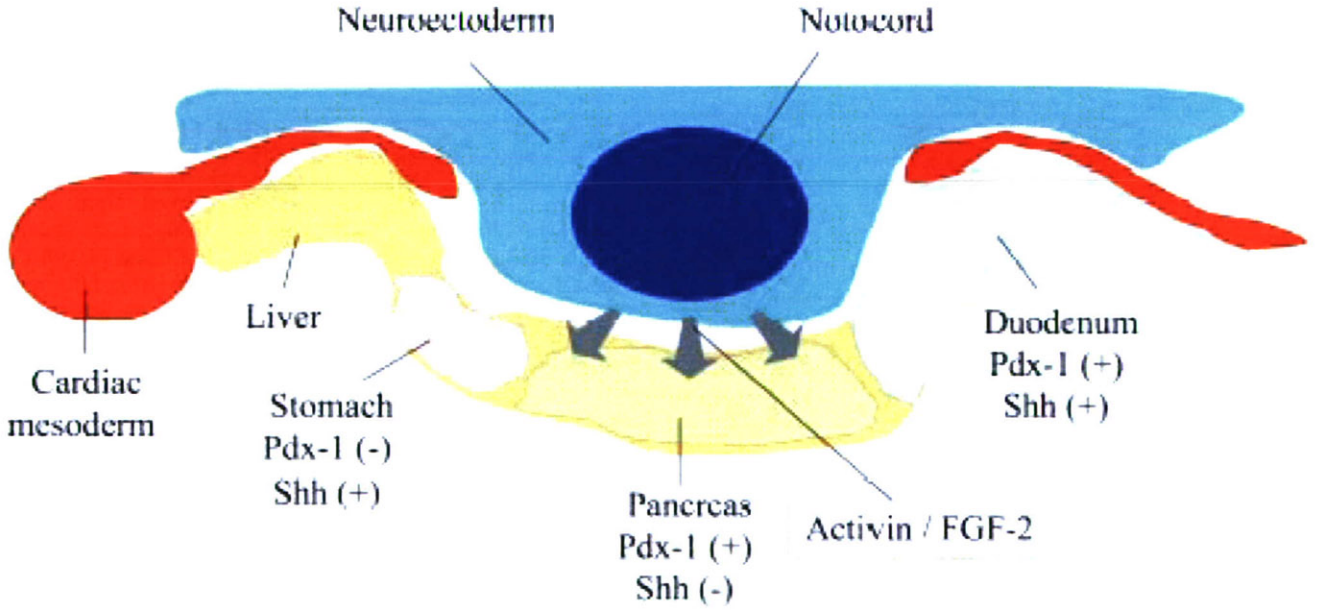

Fig. (2). Tissue-specific differentiation of the primitive pancreas.

A schematic representation shows the extracellular signals from the neighboring tissues, which regulate the tissue- and cell type-specific differentiation.